Received 4 April 2022
Revised 20 August 2022
19 September 2022
26 September 2022
Accepted 28 September 2022

A novel trussed fin-and-elliptical tube heat exchanger with periodic cellular lattice structures

Babak Lotfi
Department of Energy Sciences, Faculty of Engineering, Lund University, Lund, Sweden, and
Bengt Ake Sunden
Department of Energy Sciences, Lund University, Lund, Sweden

Abstract

Purpose – This study aims to computational numerical simulations to clarify and explore the influences of periodic cellular lattice (PCL) morphological parameters – such as lattice structure topology (simple cubic, body-centered cubic, z-reinforced body-centered cubic [BCCZ], face-centered cubic and z-reinforced face-centered cubic [FCCZ] lattice structures) and porosity value ( ) – on the thermal-hydraulic characteristics of the novel trussed fin-and-elliptical tube heat exchanger (FETHX), which has led to a deeper understanding of the superior heat transfer enhancement ability of the PCL structure.

Design/methodology/approach – A three-dimensional computational fluid dynamics (CFD) model is proposed in this paper to provide better understanding of the fluid flow and heat transfer behavior of the PCL structures in the trussed FETHXs associated with different structure topologies and high-porosities. The flow governing equations of the trussed FETHX are solved by the CFD software ANSYS CFX® and use the Menter SST turbulence model to accurately predict flow characteristics in the fluid flow region.

Findings – The thermal-hydraulic performance benchmarks analysis – such as field synergy performance and performance evaluation criteria – conducted during this research successfully identified demonstrates that if the high porosity of all PCL structures decrease to 92%, the best thermal-hydraulic performance is provided. Overall, according to the obtained outcomes, the trussed FETHX with the advantages of using BCCZ lattice structure at 92% porosity presents good thermal-hydraulic performance enhancement among all the investigated PCL structures.

Originality/value – To the best of the authors' knowledge, this paper is one of the first in the literature that provides thorough thermal-hydraulic characteristics of a novel trussed FETHX with high-porosity PCL structures.

Keywords Periodic lattice structures, Cellular materials, Heat transfer enhancement, Finned tube heat exchanger, Field synergy principle, Goodness factors

Paper type Research paper

Nomenclature

A = cross-sectional area, m^2;
A_c = minimum free-flow cross-sectional area, m^2;
A_f = fin surface area, m^2;

International Journal of Numerical Methods for Heat & Fluid Flow
Vol. 33 No. 3, 2023
pp. 1076-1115
Emerald Publishing Limited
0961-5539
DOI 10.1108/HFF-04-2022-0206

A_t = total heat-transfer surface area, m^2;
c_p = specific heat of fluid, J/kgK;
C = inertia coefficient, 1/m;
d_l = ligament diameter, m;
D_h = hydraulic diameter, m;
e = tube ellipticity ratio;
E = fan power per unit core volume, W/m^3;
f = friction factor;
F_s = fin spacing, m;
Fc = average field synergy number;
h = heat transfer coefficient, W/m^2–K;
H = cell height, m;
j = Colburn factor;
K = permeability, m^2;
l = ligament length, m;
$\dot{m}$ = mass flow rate, kg/s;
$\overrightarrow{n}$ = direction normal to wall;
Nu = Nusselt number;
p = pressure, Pa;
p' = turbulent modified pressure, Pa;
P_l = longitudinal tube pitch, m;
P_t = transverse tube pitch, m;
Pr = Prandtl number;
q'' = heat flux, W/m^2;
R_a = semi-major diameter of elliptical tube, m;
R_b = semi-minor diameter of elliptical tube, m;
Re_{D_h} = Reynolds number based on hydraulic diameter;
T = temperature, K;
u, v, w = velocity components in x, y and z-directions, respectively, m/s;
$u_{\max}$ = velocity at minimum flow cross-sectional area, m/s;
V = volume of the computational domain, m^3;
y^+ = dimensionless distance from wall; and
Z = heat transfer power per unit temperature and per unit volume, W/m^3–K.

Greek symbols

δ = fin thickness, m;
Δp = pressure drop in flow direction, Pa;
ΔT = temperature difference, K;
ε = porosity;
η_f = fin efficiency;
η_o = overall surface effectiveness;
θ = ligament inclination angle, °;
κ = turbulence kinetic energy, m^2/s^2;
λ = thermal conductivity, W/m-K;
λ_t = turbulent thermal conductivity, W/m-K;
μ = dynamic viscosity, Pa.s;
μ_t = turbulent eddy viscosity, Pa.s;
ρ = fluid density, kg/m^3;
σ = contraction ratio of cross-sectional area;

σ_κ, σ_ω = turbulent Prandtl numbers for κ and ω, respectively; and
ω = specific turbulence dissipation rate, 1/s.

Subscripts
eff = effective;
in = air-side inlet;
lm = logarithmic mean;
out = air-side outlet;
w = tube wall; and
x = local value.

Abbreviations
BC = boundary condition;
BCC = body-centered cubic;
BCCZ = *z*-reinforced body-centered cubic;
CD = computational domain;
CHX = compact heat exchanger;
CM = cellular material;
FCC = face-centered cubic;
FCCZ = *z*-reinforced face-centered cubic;
FETHX = fin-and-elliptical tube heat exchanger;
FSP = field synergy principle;
FTHX = fin-and-tube heat exchanger;
GF = goodness factor;
PCL = periodic cellular lattice;
PEC = performance evaluation criteria;
RANS = Reynolds-averaged Navier–Stokes;
SC = simple cubic;
SST = shear stress transport;
TDR = turbulent dissipation rate;
THP = thermal-hydraulic performance;
TKE = turbulent kinetic energy; and
UC = unit cell.

1. Introduction

1.1 Finned elliptical tube heat exchangers

An appreciable deal of attempts has been made over the last few decades to construct more efficient compact heat exchangers (CHXs), i.e. advanced fin-and-tube heat exchangers (FTHXs) by employing diverse thermal-hydraulic performance (THP) enhancement techniques.

When one is seeking a particular approach to intensify heat transfer rates against minimal pressure drop penalties in an industrial CHX, one will have many design challenges ahead. The main aim in ameliorating the THP of the FTHXs or in the innovative design of novel ones is to augment heat transfer between hot/cold fin-tube surfaces and the fluid flow (Mangrulkar *et al.*, 2019; Sundén, 2010).

As is well-known, extended surfaces, e.g. fins, are one of the most significant components of FTHXs, which are considered as one of the passive heat transfer enhancement methods. The most beneficial method to enhance the heat transfer on the airside of a FTHX is to optimize the fin geometry pattern. A detailed description of the heat transfer enhancement

techniques used in the FTHXs to improve THP can be found in He and Tao (2014) and Tao *et al.* (2019).

An idea to improve surface geometry of FTHXs is to use wavy (smooth wavy or herringbone wavy) fin pattern (Cheng *et al.*, 2009; Chu *et al.*, 2020; Wang *et al.*, 2002) and also interrupted fin patterns such as slit fin (Li *et al.*, 2020; Zhi *et al.*, 2021), offset-strip fin (Chennu and Paturu, 2011), louvered fin (Okbaz *et al.*, 2018; Wan *et al.*, 2020), convex-louver strip fin (DeJong and Jacobi, 1999), corrugated fin (Gholami *et al.*, 2017) and perforated fin (Fujii *et al.*, 1988). In addition, to achieve notable patterns, fins equipped with vortex generators (Chai and Tassou, 2018; Lotfi *et al.*, 2014a, 2014b, 2016a, 2016b), dimpled fin (Lotfi and Sundén, 2020b), mesh fin (Ebisu, 1999), woven wire fin (Fugmann *et al.*, 2017, 2020) and peripheral fin (Pussoli *et al.*, 2012; Ribeiro and Barbosa, 2019) can be used.

The engineering and optimization of pumping power (actually as reducing pressure drop) is of great significance in various thermal management control applications, for instance in CHX devices. Accordingly, hitherto a series of comprehensive investigations have been done to consider the thermal-hydraulic-aerodynamic performance of elliptical-shaped tube bundles of CHXs, named fin-and-elliptical tube heat exchangers (FETHXs) (Webb, 1980).

Accordingly, currently elliptical tube CHXs are widely adopted in advanced industrial heating and air-conditioning systems, to reduce the pressure loss penalty, and thus, a lower pumping cost is attained (Dogan *et al.*, 2019; Hasan and Sirén, 2004). In addition, concerning this aspect, in an innovative study, the present authors designed a new slotted-elliptical tube-bank to improve the airside THP of the FTHXs (Lotfi and Sundén, 2020a).

1.2 Periodic cellular lattice structures

By reviewing recent academic-industrial investigations in the energy transfer field, researchers' focus has changed to new innovative architectures/materials for the enhanced efficiency and improved performance in heat-exchange equipment (Li *et al.*, 2019; Singh *et al.*, 2021). Hence, cellular materials (CMs) are relatively novel materials that demonstrate commitment in a wide range of state-of-the-art mechanical/biomechanical/thermal engineering fields (Ashby *et al.*, 2000; Du Plessis *et al.*, 2022; Mahjoob and Vafai, 2008; Wan *et al.*, 2021).

Among the various CMs, it is possible to observe two kinds of CM based on topology, namely, *cell-size* (stochastic or periodic) and *pore-type* (open or closed). An illustrative diagram of the classification of CMs is shown in Figure 1 (Gibson and Ashby, 1999). It is worthwhile to note that the categorization depicted in this figure has exceptions albeit it certainly corresponds to most of the produced CMs. However, it is found that there are a lot of methods to create three-dimensional space-filling CMs such as *solid-freeform fabrication* (SFF) techniques.

During the past decades, the heat transfer phenomenon in CMs has received considerable attention. CMs have considerable applications in advanced thermal dissipation management systems, such as compact heat exchangers (Arasteh *et al.*, 2019; Buonomo *et al.*, 2020; Huisseune *et al.*, 2015; Kotresha and Gnanasekaran, 2020; Sertkaya *et al.*, 2012), thermal energy storages (Xu *et al.*, 2020; Yang *et al.*, 2019), electronics heat sinks (Li *et al.*, 2021a, 2021b), and fuel cells (Dukhan and Hmad, 2022; Vazifeshenas *et al.*, 2020), due to their high surface-to-volume ratio (SA:V) (from about 500 to over 10000 m^2/m^3), highly conducting lattice frameworks, ultra-low weight with high strength characteristics and ability to create tortuous flow-paths to promote mixing and disturbance of the fluid flow. Consequently, the three-dimensional vortices, such as *horseshoe* and *arch-shaped* vortex, caused by the tortuous path followed by a fluid passing through the CM further augment heat transfer

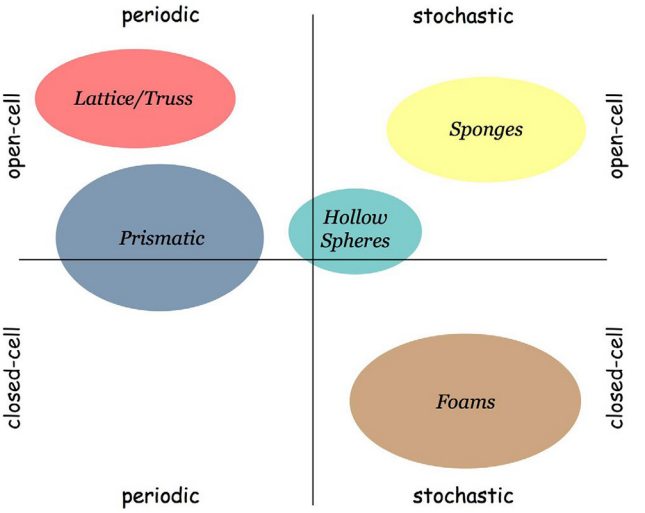

Figure 1.
Classification of CMs as a function of the topology

Source: Gibson and Ashby (1999)

(Kim *et al.*, 2005; Liang *et al.*, 2022). It should be noted that the heat transfer mechanism in CMs is complicated and not yet entirely understood due to the characteristics of flow regimes.

In most engineering applications mentioned, the awareness of the thermal transport properties and geometric-structural characteristics is of primary importance to ameliorate the THP (Chen *et al.*, 2020). The pioneering works in the development of the fluid dynamics and heat transfer study in cellular porous media in a uniform channel to include conjugate heat transfer can be traced back to Bear (1972), Collins (1976), Ettrich (2014), Nield and Bejan (2017) and Vafai and Tien (1982).

The CMs can typically be explained by a few basic key characteristics, namely, cell topology, pore size d_p, relative density ρ_r, porosity ε, ligament (strut) diameter d_l. Morphologically, the peripheries of the pore are termed ligaments with typically circular cross-section and interconnecting the vertices, forming a solid matrix which spans the whole cellular structure domain. Commonly, the porosity of CMs, such as open cell metal foam, is not less than 90% and whilst on the other hand can be as high as 98%. As pioneering investigations in CMs structure modeling, Du Plessis *et al.* (1994) and Calmidi and Mahajan (1999) proposed correlations as a function of pore diameter, porosity and ligament diameter via experimental techniques. THP of metal foam CHX results from Yu *et al.* (2006) and Nawaz *et al.* (2017) pointed out that the cell shape, pore size, and porosity strongly influence the results. For metal foam CHXs, the results reported by Sertkaya *et al.* (2012) and Huisseune *et al.* (2015) showed that metal foam CHXs cause a significant increase of the heat transfer compared to the conventional tube-bundle CHXs. Also, they found that the THP of metal foam CHXs specifically depends on the foam topology and material.

Three-dimensional periodic cellular lattice (PCL) materials are a substantial category of CMs, which have the superiority of uncomplicated topology capable of mechanical/thermal functional responses. A PCL material, unlike stochastic foam, comprises a repetitive space meshwork of longitudinal/transverse/diagonal cylindrical ligaments (or struts) of constant

cross-section, and vertices (or nodes). A vertex is a joint where two or more ligaments meet, and a ligament is a link that joins two vertices.

In general, a PCL material has a lower surface area than a stochastic foam for a given porosity. Moreover, under forced convection heat transfer conditions, the pressure drop across the PCL structure is much lower than that of the foam with a typical porosity, due to regularity in the structure. Consequently, high flow mixing occurs to improve the heat transfer performance from the solid ligaments to the convective flow. Accordingly, the heat transfer performance of PCLs is more superior compared to the stochastic foam. On the other hand, due to the structural intricacy of the solid phase of the stochastic foams, the solution of the convection–diffusion equations inside the pores are arduous to attain.

Experimental and numerical investigations on heat transfer and fluid flow characteristics of composite PCL core structures have been presented by Kim *et al.* (2005), Gao and Sun (2014) and Zhang *et al.* (2017). They manifested that the solid ligaments generate spiral and counter-rotating vortices which lead to flow mixing and hence to a high heat transfer efficiency. To support this notion, in a worthwhile review, Kim *et al.* (2005) gathered data from the immense range of resources and compared them using the thermal efficiency index $Nu/f^{1/3}$. Consequently, as seen in Figure 2, in the form-dominated flow regime (Re $>$ 1000, based on channel height), PCL materials have higher THP than other enhanced cases. This fact is ascribed to the participation of conduction through the lattice of solid ligaments in addition to forced convection.

Tian *et al.* (2004) and Krishnan *et al.* (2014) compared the overall thermal performance of PCL material against metal foams of similar porosity. They reported that the effective thermal conductivity of PCL materials is about two to three times that of metal foams.

According to the mentioned literature survey, previous investigations have proved that the high-porosity metallic foams are usually not ideal and optimal for heat-exchange systems. The available thermal-hydraulic data demonstrate that the mediocre augmentation

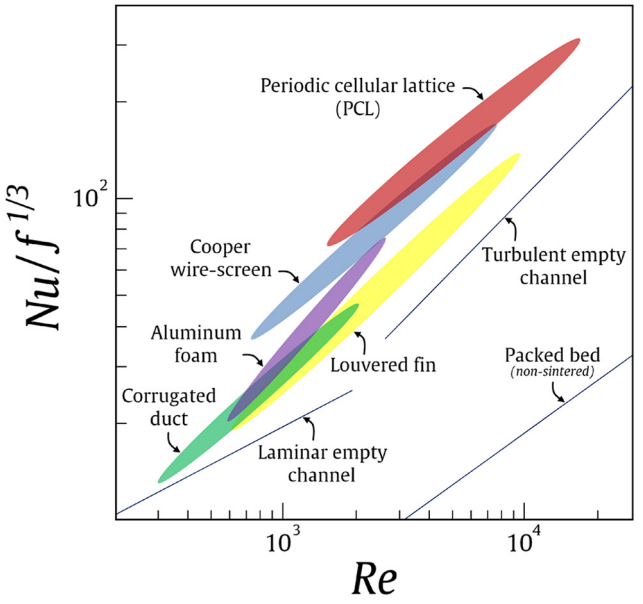

Figure 2.
THP comparisons of various heat transfer enhancement media with selected data from Kim *et al.* (2005)

in the heat transfer does not justify the considerable increase in the pressure drop, especially in the CHXs (Sertkaya *et al.*, 2012; Huisseune *et al.*, 2015; Kouidri and Madani, 2017; Han *et al.*, 2012).

Pursuant to the investigations conducted on the thermal-fluid characteristics of the PCL materials (Huu *et al.*, 2009; Kemerli and Kahveci, 2020; Lu *et al.*, 1998; Wu *et al.*, 2011), compact heat-transfer equipment consisting of three-dimensional PCL structures, such as a PCL cored sandwich panel, were found to be advantageous in thermal engineering applications.

Based on the literature survey, a regular PCL structure can be demonstrated by a finite number of polyhedral cells such as, primitive or simple cubic (SC), dodecahedron (DDH), tetradecahedron (TDH), Weaire–Phelan (WP), Kagome and X-type. Lu *et al.* (1998), Huu *et al.* (2009), Wu *et al.* (2011), Cunsolo *et al.* (2016), Kemerli and Kahveci (2020) and Yan *et al.* (2017) investigated the influences of the key geometrical features mentioned, on the heat transfer and flow characteristics of cellular media with periodic unit-cell structures formed with packed SC, DDH, TDH, WP, Kagome and X-type, respectively.

It can in general be stated that air-side fin patterns can be continuous/interrupted, or they can be PCL structures, as a "trussed fin." Accordingly, PCL materials have high porosity ($\varepsilon > 90\%$), large surface area per unit volume and offer low-pressure drop of the flow, and then have considerable potential in airside THP enhancement of a "lattice-finned tube heat exchanger."

Extended surfaces of a FTHX can as well be adjusted in an intricate network forming a fin system. Trussed fin patterns can have diverse architectures as was previously investigated by Bejan (1997) and Almogbel and Bejan (2000). In their studies, they modeled heat transfer via tree-like fin networks, a primary fin with secondary fins attached to it. Based on the results of a numerical study by Khaled (2007), a variation of the fin augmentation technique, termed "hairy fin system" was proposed. It was composed of a basic rectangular fin with many slender secondary bars attached on its primary fin surface.

It has been apparent from the foregoing literature review that no related comparative investigation of three-dimensional numerical simulation analysis for trussed FTHX with various high-porosity PCL core structures has been published. Besides, most of the research works were related merely to porous media heat sink consisting of a PCL-cored sandwich panel.

The purpose of the present work is to introduce five types of PCL structures built from regular unit cells (UCs) – simple cubic (SC), body-centered cubic (BCC), reinforced body-centered cubic with vertical ligaments (BCCZ), face-centered cubic (FCC) and reinforced face-centered cubic with vertical ligaments (FCCZ) with different porosities of 92% and 98%, for application in a novel FETHX. Furthermore, the conjugate heat transfer problem and the influences of UC configuration and porosity on each of the PCL structures on the thermal-hydraulic performance of a trussed FETHX are explored.

2. Model description and mathematical formulations

2.1 Periodic-lattice unit cell model specifications

Figure 3 shows a schematic illustration of 3D-CAD space-filling lattice models of five diverse types of periodic equal-sized cubic cells considered in this study, namely, SC, BCC, BCCZ, FCC and FCCZ, with controllable geometric parameters.

The simple (or primitive) cubic UC structure has one vertex at each of its eight corners [see Figure 3(a)]. The UC structure of BCC has one central vertex, from which eight diagonal cylindrical ligaments extend to the UC corners. The UC structure of BCC consists of eight ligaments having the same length [see Figure 3(b)]. The UC structure of BCCZ (or a

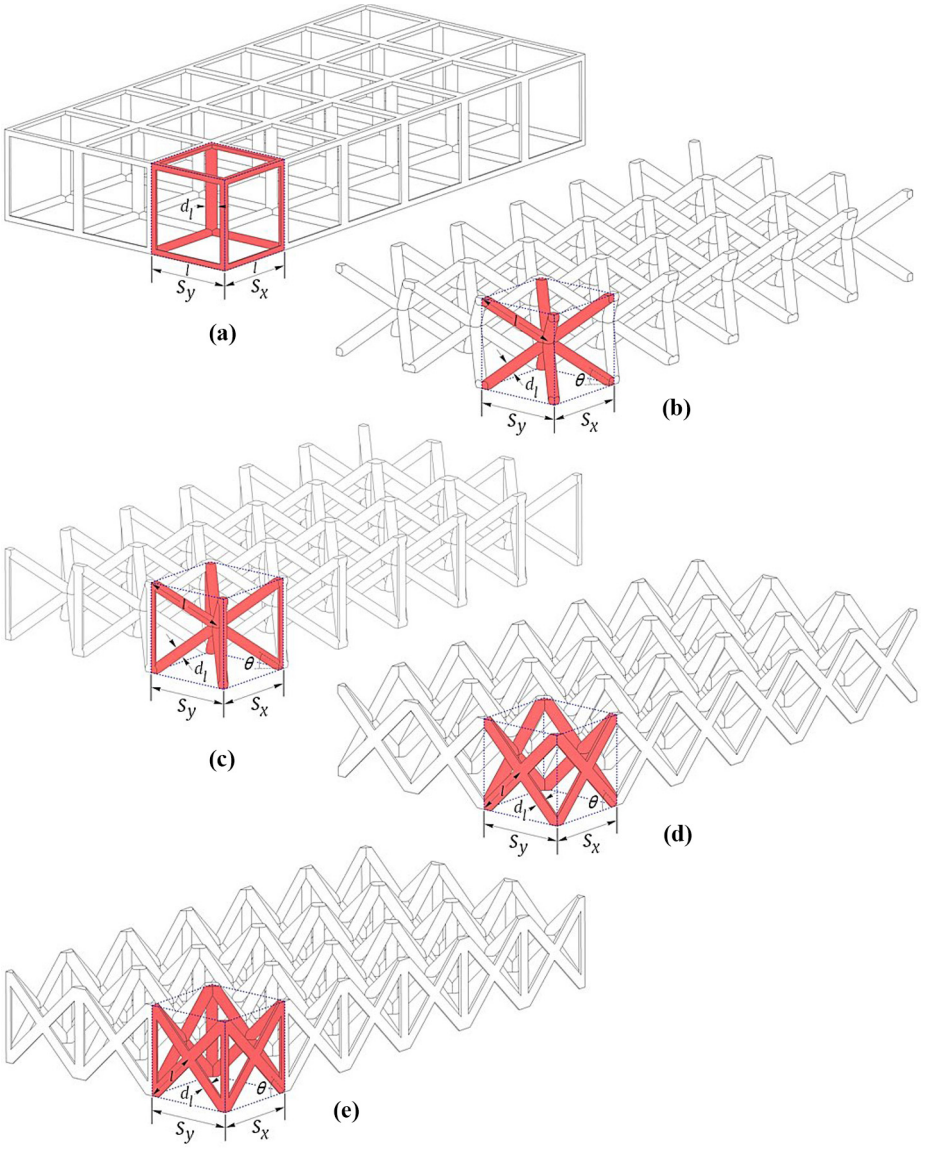

Notes: (a) SC; (b) BCC; (c) BCCZ; (d) FCC; (e) FCCZ

Figure 3.
Geometric parameters of single-layered PCL structures in the *in-plane* direction with five 3D regular unit-cells

reinforced BCC) is similar to the BCC structure, but with four additional vertical ligaments along the four vertical edges of the cell as depicted in Figure 3(c). The UC structure of FCC has two crossed ligaments on each of the vertical faces [see Figure 3(d)]. The UC structure of FCCZ (or a reinforced FCC) is a variant of FCC with four vertical ligaments along the *z*-axis as seen in Figure 3(e).

The PCL structure can be parameterized by ligament diameter d_l, length of ligament l (from vertex center to vertex center), ligament inclination angle θ, UC height H, and the dimension S represents the UC width and length. For this study, all the dimensions of the cubic UCs are equal for all investigated configurations (i.e. $S_x = S_y = H$). Figure 3 describes all the relevant controllable geometric parameters of the PCL structure. The cross-section form of each ligament is assumed to be circular, having a constant diameter. The diameter and length of the ligament are dependent variables and will be determined only by the porosity of the lattice structure and cell size.

For PCL structures built from UCs, the volumetric porosity of their CAD models was defined using the following expression:

$$\text{Porosity} \quad \varepsilon = 1 - \frac{V_{lig}}{V_{uc}} \tag{1}$$

where V_{lig} is the volume of the CAD lattice ligaments and V_{uc} is the overall volume restricted by the exterior periphery. Indeed, according to the stated relationship, the porosity ε can be quantified by the relative volume $V_{rel} = V_{lig}/V_{uc}$, i.e. related to the UC dimensions by:

$$V_{rel} = C\left(\frac{d_l}{l}\right)^2 \tag{2}$$

where d_l/l is the ligament aspect ratio and C is a structural constant that depends on the details of the UC structure. The porosity relations of lattice structures with different types of repeating UCs are listed in Table 1 (Hooman *et al.*, 2012; Hammetter *et al.*, 2013; Umer *et al.*, 2018). Thus, for a given porosity ε, one can achieve the ligament diameter of each UC.

Cell shape	Porosity ε	
Simple cubic (SC)	$1 - \left\{\frac{3\pi}{4}\left(\frac{d_l}{l}\right)^2\right\}$	(3)
Body-centered cubic (BCC)	$1 - \frac{\pi}{2\cos^2\theta \sin\theta}\left(\frac{d_l}{l}\right)^2 = 1 - \frac{3\sqrt{3}\pi}{4}\left(\frac{d_l}{l}\right)^2, \ for\ \theta = \tan^{-1}\frac{\sqrt{2}}{2}$	(4)
Reinforced body-centered cubic (BCCZ)	$1 - \frac{\pi\left(1+\frac{1}{4}sin\theta\right)}{2\cos^2\theta sin\theta}\left(\frac{d_l}{l}\right)^2 \approx 1 - \frac{6\sqrt{6}}{\pi}\left(\frac{d_l}{l}\right)^2, \ for\ \theta = \tan^{-1}\frac{\sqrt{2}}{2}$	(5)
Face-centered cubic (FCC)	$1 - \frac{\pi}{\sin^3\theta}\left(\frac{d_l}{l}\right)^2 = 1 - 2\sqrt{2}\pi\left(\frac{d_l}{l}\right)^2, \ for\ \theta = 45^\circ$	(6)
Reinforced face-centered cubic (FCCZ)	$1 - \frac{\pi(4+sin\theta)}{4\sin^3\theta}\left(\frac{d_l}{l}\right)^2 = 1 - \pi\left(2\sqrt{2}+\frac{1}{2}\right)\left(\frac{d_l}{l}\right)^2, \ for\ \theta = 45^\circ$	(7)

Source: Hooman *et al.* (2012), Hammetter *et al.* (2013), Umer *et al.* (2018)

Table 1.
List of volumetric porosity formulas for equilateral (regular) periodic lattice structures

2.2 Trussed fin-and-elliptical tube heat exchanger geometry model

The three-dimensional schematic view of the geometrical model and corresponding computational domain (CD) with boundary conditions (BCs) of the trussed FETHX with single-layered PCL core structure considered in the current study are given in Figure 4.

A single cell of the above-mentioned unit cells (SC, BCC, BCCZ, FCC and FCCZ) is uniformly distributed in the *in-plane* direction with patterning distance determined by $S_x = H$. It is attached on the primary plain fin surface. Thus, the PCL core is located between adjacent plain fins. Accordingly, in the SC, BCC, BCCZ, FCC and FCCZ lattice structures, the vertices are attached on the lower and upper fin surfaces. For the BCC, BCCZ, FCC and FCCZ lattice structures, in addition to attaching the vertices to the fin surfaces, there also exist vertices on the middle plane between the two adjacent fin surfaces.

To assess the amelioration of novel FETHX using PCL core structures, the present three-dimensional numerical study investigates the usage of elliptical tubes in a staggered arrangement. The detailed geometrical parameters of the FETHX are summarized in Table 2. Figure 4 also depicts the view of the actual CD and the prescribed BCs, where the upstream and downstream regions of the computational domain are not shown completely due to space constraint of this paper.

The adjacent two primary fins' centric surfaces are picked as the lower and upper of the CD boundaries. The actual CD was extended 5 and 20 times relative to the F_s for the entrance and exit region, respectively, to maintain a uniform inlet velocity and to minimize and avoid influences of flow disturbance and recirculation from the outlet. The definition of the local coordinate system, (x, y, z), covers the streamwise, spanwise, and normal coordinates, respectively. The central CD was modelled in the *CATIA® V6* (*Dassault Systèmes, Inc.*) as an authentic three-dimensional model of a novel FETHX with five distinct configurations of high-porosity PCL core structures, and built-in three-staggered rows of elliptical tubes.

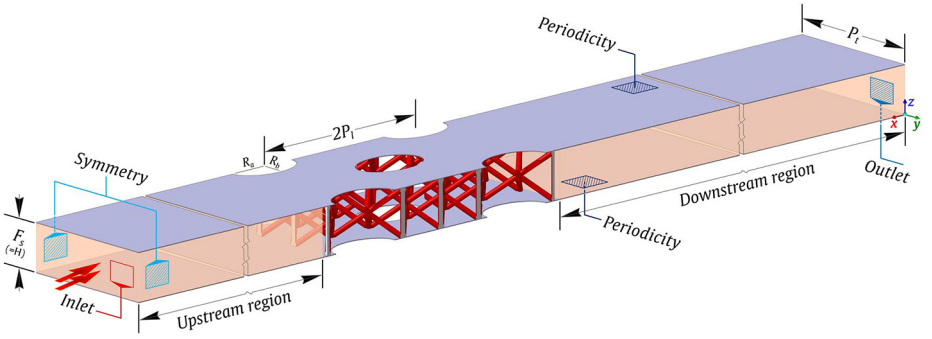

Figure 4.
3 D schematic representation of the geometric details of a trussed FETHX with PCL structure and BCs for the CD

Parameter	Value
Ellipticity ratio, $e = R_b/R_a$	0.65
Longitudinal tube pitch, P_l	16.8 mm
Transverse tube pitch, P_t	25.2 mm
Plain fin thickness, δ	0.2 mm
Fin space, F_s	8.6 mm

Table 2.
Geometrical parameters of the FETHX

2.3 Flow governing equations and turbulence modeling

In numerical solutions of flow and conjugate heat transfer problems, the selection of flow governing equations performs a key role because the vorticity flow physics are considerably influenced by the governing equations.

Three-dimensional computational fluid dynamics (CFD) simulations of the thermal-hydraulic characteristics in the trussed FETHX with PCL structures are carried out by an eddy-viscosity turbulence model. For the present study, the assumptions of the considered fluid properties are the same as those used by Lotfi *et al.* (2016b) and Lotfi and Sundén (2020b). By applying vectorial notation, the system of the three-dimensional flow governing equations used to describe the steady turbulent fluid flow and heat transfer for the fluid domain can be formulated as in Table 3.

The results presented in Fu *et al.* (2017), Fugmann *et al.* (2017) and Välikangas *et al.* (2018) showed that the recommended turbulence model to predict fluid-dynamic behavior of FTHX with *flow manipulators or turbulators*, for cases with $\mathrm{Re}_{D_h} \geq 500$, is the *Shear Stress Transport* (*SST*) $\kappa - \omega$ turbulence model, that was developed by Menter (1994). On the other hand, it was found that the turbulence intensity can be enhanced by up to 80%, when the airflow is passing through the CM interior (Hall and Hiatt, 1996). Similarly, Moon *et al.* (2016) and Yu *et al.* (2018) used the *SST* $\kappa - \omega$ turbulence model for simulation of detailed flow and heat transfer in regular PCL structures.

This investigation uses the Menter *SST* $\kappa - \omega$ turbulence model to accurately predict flow characteristics. Indeed, the Menter *SST* $\kappa - \omega$ turbulence model is a precise and robust hybrid model, using a *Low-Reynolds* $\kappa - \omega$ turbulence model near the solid walls and a $\kappa - \varepsilon$ turbulence model in free shear layers and boundary layer edges. In the Menter *SST* $\kappa - \omega$ turbulence model, the transport formulations for the TKE (turbulent kinetic energy, κ) and the TDR (turbulent dissipation rate, ω), are defined as in Table 3. A detailed interpretation of the closure coefficients and blending functions appearing in the standard *SST* $\kappa - \omega$ model equations can be found in ANSYS CFX (2018) and Menter (1994).

2.4 Boundary conditions and computational procedure

A summary of the BCs employed in the CD can be observed in Figure 4. Hereupon, the indispensable BCs are described for regions as follows:

(1) Inlet: $u = u_{in}$ *const.*, $v = w = 0$, $T = T_{in} = 343K$, turbulence intensity level = 5%

(2) Outlet: *zero streamwise gradient for all the variables*

Item		Equation expression	
Conservation equations	Continuity equation	$\nabla \cdot \vec{u} = 0$	(8)
	RANS equation	$\nabla \cdot (\rho \vec{u} \otimes \vec{u}) - \nabla \cdot \left(\mu_{eff} \nabla \vec{u}\right) = -\nabla p' + \nabla \cdot \left(\mu_{eff} \nabla \vec{u}\right)^T$	(9)
	Energy equation	$\rho c_p \nabla \cdot (\vec{u} T) = \nabla \cdot (\lambda_{eff} \nabla T)$	(10)
SST $\kappa - \omega$ turbulence equations	TKE equation	$\rho \nabla \cdot (\kappa \vec{u}) = \nabla \cdot \left[(\mu + \mu_t \sigma_\kappa) \nabla \kappa\right] + \tilde{G}_\kappa - Y_\kappa$	(11)
	TDR equation	$\rho \nabla \cdot (\omega \vec{u}) = \nabla \cdot \left[(\mu + \mu_t \sigma_\omega) \nabla \omega\right] + G_\omega - Y_\omega + D_\omega$	(12)

Notes: $\vec{u}$: fluid velocity vector; μ_{eff}: effective viscosity, $\mu_{eff} = \mu + \mu_t$; λ_{eff}: effective thermal conductivity, $\lambda_{eff} = \lambda + \lambda_t$; $\tilde{G}_\kappa, G_\omega$: generation term of κ and ω, respectively; Y_κ, Y_ω: dissipation term of κ and ω, respectively; D_ω: cross-diffusion term

Source: ANSYS CFX (2018), Menter (1994)

Table 3. Summary of the flow governing equations for 3D-CFD simulations, with *SST* $\kappa - \omega$ turbulence model

(3) Elliptical tube wall surfaces: *no-slip conditions*, $T = T_w = 293K$
(4) PCL structure surfaces: *no-slip conditions*
(5) Top and Bottom sides (*xy*-plane):
    - At extended regions: *periodic conditions*
    - At primary fin surfaces: *no-slip and adiabatic conditions*
(6) Front and Back sides (*xz*-plane):
    - At fluid and extended regions: *symmetric conditions*
    - At trussed fin surfaces: *no-slip and adiabatic conditions*
(7) Solid–fluid interface: $T_{solid} = T_{fluid}$, $-\lambda_{solid}\left(\partial T_{solid}/\partial \overrightarrow{n}\right) = -\lambda_{fluid}\left(\partial T_{fluid}/\partial \overrightarrow{n}\right)$

The stipulated governing equations of the trussed FETHX are solved by the CFD software *ANSYS CFX® 19.2* developed by *ANSYS Inc.* (ANSYS CFX, 2018). More details about the CFX numerical core algorithm applied to the 3 D thermal-hydraulic numerical simulations in this paper can be found in ANSYS CFX (2018) and Lotfi and Sundén (2020b), and will not be restated here for brevity. The convergence criterion for all variables is that the maximum normalized residual value should be less than 10^{-8}.

3. Computational simulation methodology

3.1 Assessment parameters

The essential target of the present study is to simulate and predict the air-side thermal-hydraulic characteristics in a novel trussed FETHX with five types of PCL core structures. The evaluation parameters applied in the investigation are summarized in Table 4.

Some advanced passive heat transfer enhancement methods have managed to cut down to certain extent not only comparative energy consumption (CEC) but also the cost of equipment in thermal industries. Therefore, to be aware of the essence of these advanced enhancement techniques from the standpoint of temperature and velocity fields, Guo *et al.* (1998) were the first to propose the *field synergy principle* (FSP) concept for convective heat transfer intensification. Fluid flow FSP for convective heat transfer explains that when the direction of flow velocity is closer to the direction of the temperature gradient, this might mean opportunity for heat transfer augmentation.

However, because of application conditions (e.g. thermal boundary condition and flow regime) on field synergy performance, utilization of the FSP has some constraints (Yu *et al.*, 2018; Zhao *et al.*, 2020). For instance, it has been shown that in a turbulent flow regime over complex boundary geometries, the synergy degree could not consider the turbulent diffusion effect (Zhu and Zhao, 2016). According to the literature survey, it is found that the dimensionless synergism parameter, i.e. *field synergy number*, exhaustively embodies the FSP, is more proper for providing a criterion to assess the synergy degree, especially in a complicated region with turbulent flow (Guo *et al.*, 2011; Yu *et al.*, 2018).

In the entire volume of the CD, the average field synergy number *Fc* can be specified under dimensionless variables form by introducing the characteristic length D_h ($D_h = 4\,V/A_t$) as:

$$Fc = \iiint_V (\overline{u} \cdot \overline{\nabla T}) d\overline{V} \tag{26}$$

where $\overline{u} = u/u_{frontal}$, $\overline{\nabla T} = \nabla T / \left[\left(T_{airflow,m} - T_{fin,m}\right)/D_h\right]$ and $d\overline{V} = dV/V$. The more thorough explanation of the field synergy number can be found in the studies by Guo *et al.* (1998, 2005).

Table 4.
Summary of the performance and evaluation parameters

Appraisals parameter	Equation expression	
Reynolds number	$\mathrm{Re}_{D_h} = \rho u_{max} D_h / \mu$	(13)
▶ Hydraulic diameter	$D_h = 4V/A_t$	(14)
▶ Maximum air velocity	$u_{\max} = u_{frontal}\left(A_{forntal}/A_c\right)$	(15)
Overall average heat transfer coefficient	$h = \dot{m} c_p (T_{in} - T_{out}) / \eta_o A_t \Delta T_{lm}$	(16)
▶ Outlet bulk temperature	$T_{out} = \iint_{out} u_x T \mathrm{d}A_{out} \Big/ \iint_{out} u_x \mathrm{d}A_{out}$	(17)
▶ Logarithmic mean temperature	$\Delta T_{lm} = \{(T_{in} - T_w) - (T_{out} - T_w)\} / \ln\{(T_{in} - T_w)/(T_{out} - T_w)\}$	(18)
▶ Overall air-side surface effectiveness	$\eta_o = 1 - \left(A_f / A_t\right) \cdot \left(1 - \eta_f\right)$	(19)
Average Nusselt number	$Nu = \iint_{A_t} Nu_x \mathrm{d}A_t \Big/ \iint_{A_t} \mathrm{d}A_t$	(20)
▶ Streamwise local Nusselt number	$Nu_x = \{\left(q_x^{''} / T_{airflow,x} - T_{fin,x}\right) D_h\} / \lambda$	(21)
Colburn factor	$j = Nu / \mathrm{Re}_{D_h} \cdot Pr^{1/3}$	(22)
Friction factor	$f = \left(2\Delta p / \rho u_{\max}^2\right) \cdot \left(A_c / A_t\right)$	(23)
Isothermal heat transport density	$Z = \eta_o h (4\sigma / D_h)$	(24)
Pumping power density	$E = (\dot{m} \Delta p / A_t \rho)(4\sigma / D_h)$	(25)

Notes: $u_{frontal}$: frontal velocity (inlet airflow velocity), vary from about 0.6 m/s to 3.4 m/s yielding Re_{D_h} range from 500 to 3000; η_f: fin efficiency, determined by the approximation method proposed by Schmidt (1949) and an iterative calculation; $q_x^{''}$: span-averaged local heat flux; $T_{airflow,x}$: mass-weighted average air temperature of the cross-section; $T_{fin,x}$: span-averaged local fin temperature

Clever combinations of enhancement techniques used in compact FTHXs, i.e. *extended surfaces plus flow manipulators*, to improve the thermal performance have been developed enormously over the past years. The intention of compact FTHX design and development is to achieve a superior heat transfer performance combined with a pressure loss as low as possible. As is well-known, the fluid pressure drop will rise while the heat transfer is augmented. Consequently, indispensable to establish appropriate *performance evaluation criteria* (PEC), namely, principal goodness factors (GFs) (Shah, 1978), to assess the THP of these employed techniques to select the most appropriate one for given operating conditions. In accordance with the assumption of constant properties, the PECs' approach is considered, namely, *flow area GF* ($j/f^{1/3}$ *vs*. Re_{D_h}) and *core volume GF* (Z vs E), suggested by Webb and Kim (2005) and Kays and London (1950), respectively (see the equations in Table 4). The more thorough explanation of the utilization of GFs in the evaluation of CHXs can be found in Lotfi and Sundén (2020b).

3.2 Grid generation and grid independence test

The high precision of the CFD solutions relies on the topology and density distribution of the grid in the CD. For all CFD-simulation cases, a multi-block hybrid grid topology (i.e. unstructured tetrahedral/structured hexahedral) is applied to discretize the entire CD. It is generated using the software code *ANSYS ICEM CFD® 19.2* (*ANSYS, Inc.*) (ANSYS ICEM, 2018).

To have reasonable accuracy of the three-dimensional numerical simulation results, the grid close to the PCL structures and elliptical tube walls is refined to enable resolution of the horseshoe/longitudinal vortices where high gradients are expected, as demonstrated in Figure 5. With the intention to validate the grid independence of the numerical solution, four various grid systems, including about 6.14 million, 7.51 million, 8.79 million and 9.18 million cells were selected and assessed at $\mathrm{Re}_{D_h} = 3000$ for the FCCZ lattice structure for the 92% porosity case.

The predicted the friction factor f and average Nusselt number Nu for the four grid systems are provided in Table 5. The relative deviations of the friction factor f and the average Nusselt number Nu between the 9.18 million grid cells and the 8.79 million grid cells are less than 1% and 1.2%, respectively, as shown in Table 5. Accordingly, to keep a trade-off between simulation economics and prediction accuracy, the adopted grid cells number in the CD is about 8.79 million. Similar grid refinement trials were conducted for the subsequent simulation cases as well. In addition, for the purpose to ensure computational

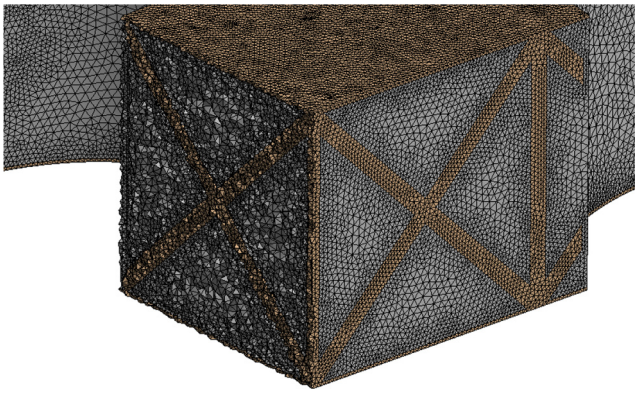

Figure 5.
The representative grid of the actual computational domain for the FCCZ lattice structure

accuracy, all grids close to the walls and trussed fin surfaces are extremely dense and meet the condition $y^+ \leq 1$ (ANSYS CFX, 2018), for all Reynolds numbers investigated.

3.3 Numerical CFD validation

To validate the precision of the present CFD-simulation method, preliminary computational results for a FTHX were compared with the comprehensive experimental data obtained by Wang *et al.* (2000). To predict the fluid flow and heat transfer characteristics in the FTHX, three various models are considered in this section of the present study, namely, a *laminar* model, the *Re-Normalization Group* $\kappa - \omega$ turbulence model (Yakhot *et al.*, 1992) and the *SST* $\kappa - \omega$ turbulence model. As shown in Figure 6, the maximum difference between the numerical results obtained from the *SST* $\kappa - \omega$ model and the experimental data for Colburn j factor and friction factor f were found to be less than 10% and 4%, respectively. This good agreement demonstrates the reliability of the computational model. Therefore, in the present investigation, the *SST* $\kappa - \omega$ turbulence model is chosen for simulation of the flow behavior in the fin channel with PCL structures.

In fact, no direct experimental results, or even no relevant experimental research studies, about the fluid flow and heat transfer characteristics of trussed FETHXs with PCL core structures are available. However, to further validate the reliability of the implemented CFD turbulence model, numerical results of pressure drop were evaluated by simulations of fluid flowing through the PCL material.

As is well-known, generally, abundant experimental investigations on CMs, e.g. metal foams, have been carried out and accordingly many pressure drop correlations have been derived (Edouard *et al.*, 2008; Bracconi *et al.*, 2019). Pressure drop can be estimated through the Darcy's model and Forchheimer-extended Darcy's model established for CMs. It should be noted that application of the Darcy model is only appropriate for low-velocity regimes ($\mathrm{Re} < 0.1$) in the CM with low permeability. On the other hand, at higher Reynolds numbers the viscous shear force and viscous dissipation effect become appreciable (Vafai and Tien, 1982), and hence, the pressure drop can be somewhat more accurately described by the Forchheimer-extended Darcy model equation:

$$\frac{\Delta p}{\ell} = \frac{\mu}{K} u + C \rho u^2 \tag{27}$$

where K is the permeability and C is the inertial coefficient. This might be more substantial near the boundary and in high-porosity CM. These coefficients are not actually constants; instead, they are entirely dependent on the CM geometrical characteristics and can be obtained only from several experimental results.

Over the past decades, considerable experimental studies have been performed to establish on the pressure drop correlations of high-porosity CMs. However, despite abundant investigations on CMs and the wide difference of CM geometrical parameters, the pressure drop correlations obtained are also diverse and none of them exhibits universal applicability so far (Dietrich, 2012).

Table 5. Grid independence study

Grid no.	6.14 million	7.51 million	8.79 million	9.18 million
Nu	83.855	88.626	90.021	90.713
f	0.521	0.441	0.425	0.420

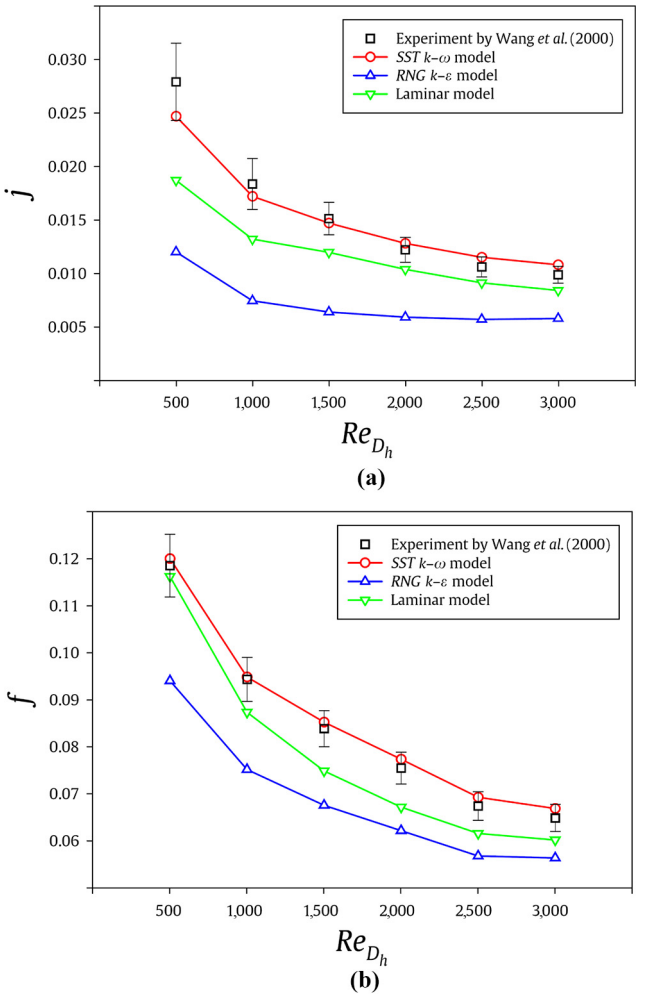

Figure 6.
Experimental-numerical comparison of Colburn *j* factor and friction factor *f* for model validation

To scrutiny the precision of the CFD simulation outcomes in this study, the pressure drop correlation for various geometrical parameters proposed by Dietrich (2012) is considered. It is noteworthy that Dietrich's correlation was derived based on more than 2,500 experimental data, within an error range of ±40% (Dietrich, 2012). To this end, simulation of the air-side performance is carried out in a channel filled with the *tetrakaidecahedron* PCL model, which can be considered as an ideal CM, according to the configuration and conditions provided in Dietrich *et al.* (2009). The pressure drop per unit length ($\Delta p/\ell$) as a function of inlet airflow velocity obtained from the present CFD simulation is compared with the Dietrich's correlation (Dietrich, 2012), as presented in Figure 7. As expected, the numerical simulation results correspond reasonably well with the pressure drop correlation established by Dietrich.

4. Computational results and discussion

4.1 Flow pattern and secondary flow vortices

Considering the heat transfer augmentation in advanced trussed FETHXs with PCL materials, it is of interest to understand the profound heat transfer enhancement mechanisms. Thus, the details of flow structure and influences of PCL geometric parameters affecting heat transfer performance on fin surfaces are compared. Indeed, such phenomena can be useful for researchers to develop more effective PCL materials in thermal industries.

Depictions of flow patterns including the various types of secondary flow vortices, are displayed in Figure 8. Predicted three-dimensional trajectories of the airflow close to trussed fin surfaces induced by the PCL core structures with 92% porosity are presented at $\mathrm{Re}_{D_h} = 3000$. As expected, in comparison FETHX without PCL, the PCL core structures change the main flow pattern and promote the turbulent flow intensity. Due to the presence of the longitudinal/transverse/diagonal ligaments and the structure vertices, the developed boundary layer tends to be broken up and rolled up in front of the junction of the PCL vertex and fin surface. It is clearly revealed that the airflow behaviors at the stagnation and downstream zones around the elliptical tube are completely changed and the airflow passing through the PCLs presents more complex flow patterns. The great fluid flow resistance adjacent to the PCL vertices could be causing high swirling velocity secondary flow, which interacts with the boundary layer on the fin surfaces and the PCL ligaments. This may lead to a considerable increase of the heat transfer performance. Also, *horseshoe* and *arch-shaped* vortex structures are observed along the upstream region of the PCL ligaments and vertices generating regions of reversed flow (i.e. flow recirculation and reattachment to forward flow). This leads to increased turbulence intensity. However, owing to the difference of the forms of the PCL vertices in SC, BCC, BCCZ, FCC and FCCZ lattice structures, the swirl flow around the vertices representations various complex patterns. Accordingly, as air is flowing over the central vertices, a pair of counter-rotating vortices is created in the wake regions behind the vertices. It is worthwhile to mention that more detailed explanation of these vortex structures across the PCL structure was addressed by Kim *et al.* (2005).

Owing to the distinction of the ligament configurations in the PCL structures, i.e. having downward and upward slopes along the main flow direction, the swirling flow around the ligament depicts various patterns near the upper and lower fin surfaces. In front of each

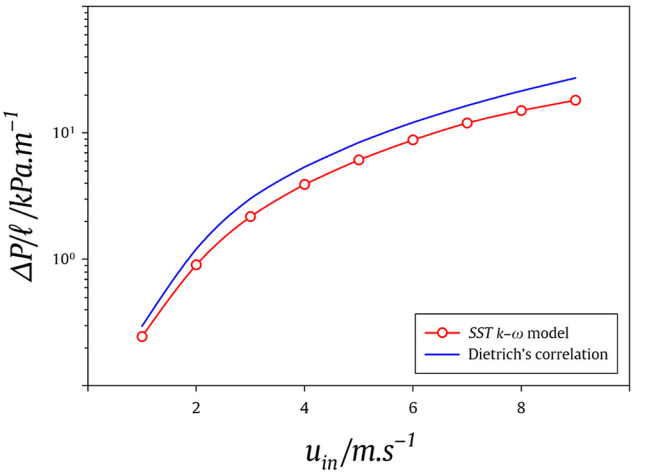

Figure 7.
Comparison of the Dietrich's pressure drop correlation (Dietrich, 2012) and the numerically simulated data from the tetrakaidecahedron PCL model with $\varepsilon = 92\%$

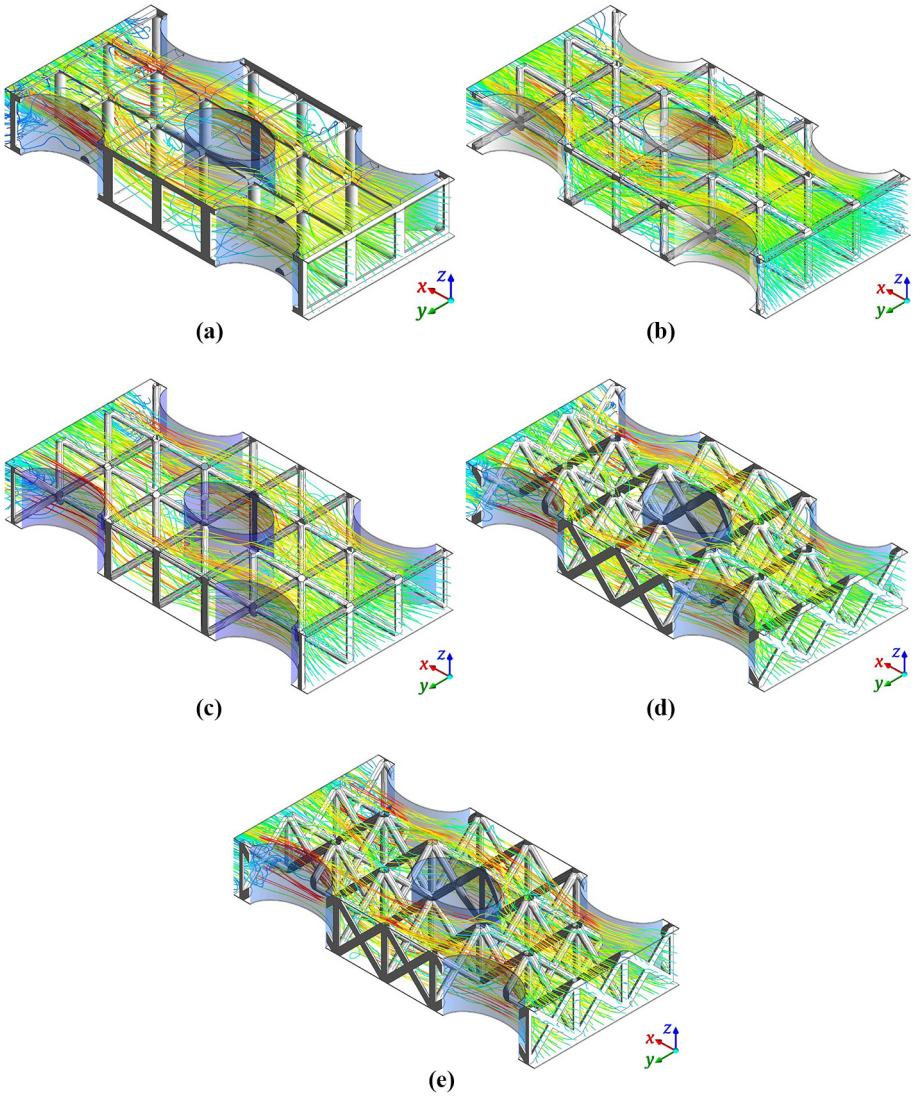

Notes: (a) SC; (b) BCC; (c) BCCZ; (d) FCC; (e) FCCZ

Figure 8.
Comparison of flow patterns indicated by three-dimensional trajectories close to trussed fin surfaces induced by PCL structures with $\varepsilon =$ 92%, at $\mathrm{Re}_{D_h} = 3000$

transverse/diagonal ligament, as the fluid is passing the ligaments, the fluid is forced to flow upward owing to the high-pressure gradient induced by the inclination of the ligament. Also, flow separation occurs at the downstream side of each of these ligaments. Therefore, a pair of counter-rotating streamwise vortices appears behind the ligaments. This phenomenon is clearly shown in the flow patterns as displayed in Figure 8. This means that heat transfer is considerably augmented by increasing the airflow mixing and disturbance

effects induced by the PCL ligaments and vertices as well as by the high thermal conductivity through the metallic ligaments.

To better reveal the heat transfer augmentation mechanisms for all the enhanced cases PCL structures, Figures 9 and 10 delineate the CFD-simulated predictions of the streamlines overlaid on the temperature contours for the five enhanced cases with 92% and 98% porosity, respectively. The contours are shown in the three vertical cross-section passages through the mid-vertices ($x_i = 7\,R_a$, $x_{ii} = 11\,R_a$ and $x_{iii} = 15\,R_a$ from the inlet of the model) just after the first, second and third tube rows, at $\mathrm{Re}_{D_h} = 3000$.

The important phenomenon to notice is the substantial influence of the PCL porosity on the fluid flow characteristics. As the airflow enters the PCL material, it accelerates substantially, especially for the lowest porosity case ($\varepsilon = 92\%$) which has a smaller pore size. It is clear from this figure that the lowest porosity case, ($\varepsilon = 92\%$), provides the highest disturbances with vortices formed downstream of the PCL ligaments, whereas the highest porosity case, ($\varepsilon = 98\%$), provides an almost uniform velocity distribution with the least vorticity intensity downstream of the PCL ligaments and vertices.

From the vertical sections depicted in Figure 9, it is evident that in the BCCZ lattice structure with the porosity $\varepsilon = 92\%$ stronger counter-rotating vortices adjacent to the end-wall are produced and the number of vortices is higher than for the other PCL structures, which leads to a higher heat transfer for this porosity. As shown in Figure 10, the FCCZ lattice structure with the porosity $\varepsilon = 98\%$ provides the highest vortex intensity and the velocity gradient is higher than for the other PCL structures. This causes better thermal performance.

Compared to all the enhanced cases, the BCCZ lattice structure and the FCCZ lattice structure have vertices with five overlapping ligaments on the fin surface, which induces more irregular vortices and promotes flow mixing. In these two lattice structures, due to the

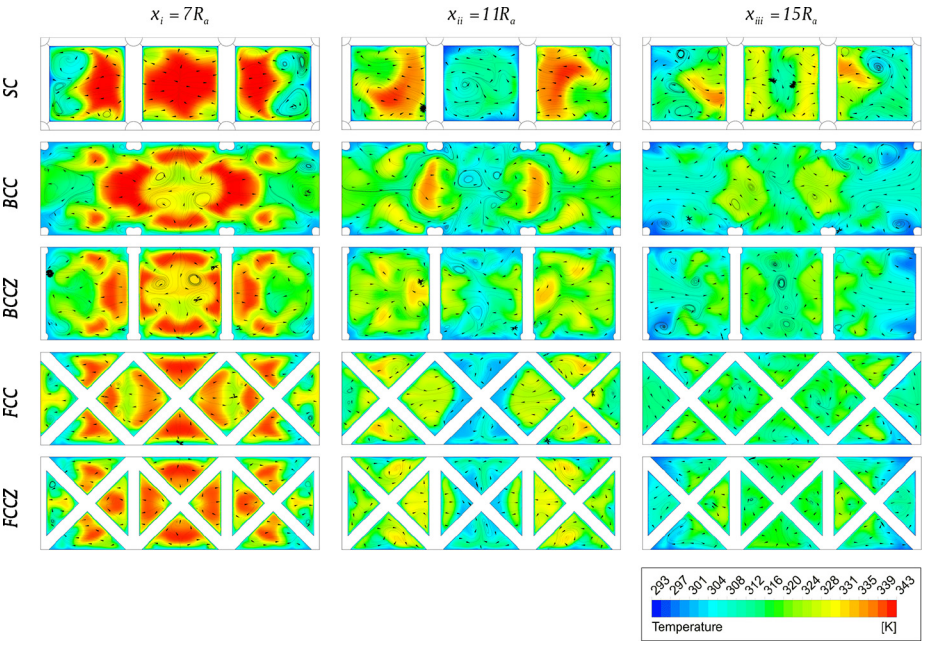

Figure 9.
Streamlines and temperature contours in transverse planes at $\varepsilon = 92\%$, $\mathrm{Re}_{D_h} = 3000$

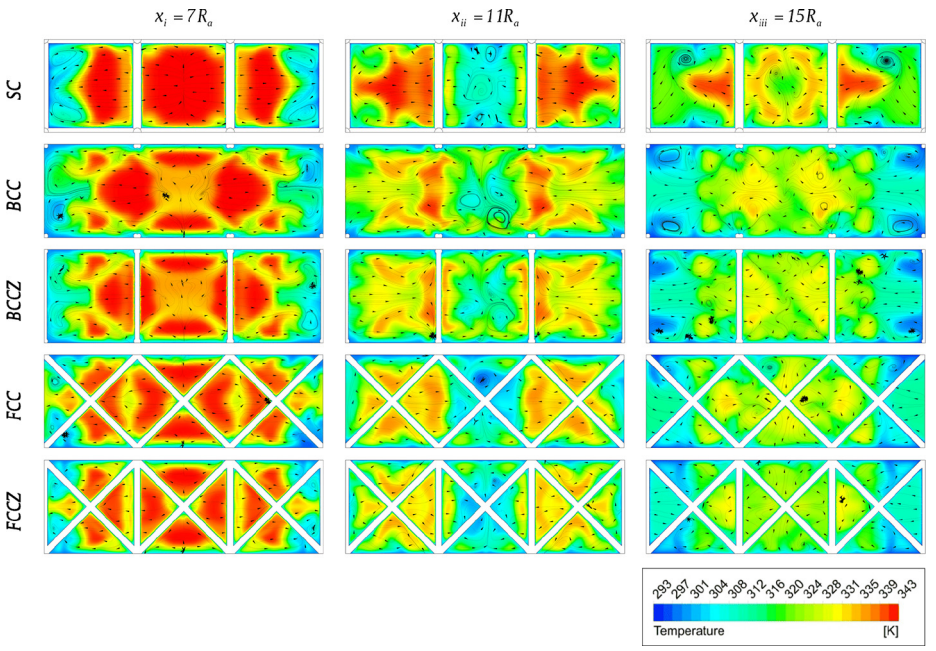

Figure 10. Streamlines and temperature contours in transverse planes at $\varepsilon = 98\%$, $\mathrm{Re}_{D_h} = 3000$

presence of vertical ligaments along the *z*-axis, a strong horseshoe vortex is formed around the vertical ligament and fin junction, and a pair of counter-rotating streamwise vortices appears downstream of each ligament.

4.2 Local analysis of the flow and heat transfer fields

To better illustrate the detailed internal flow patterns and their effect on heat transfer characteristics, Figure 11 presents a comparison of the velocity streamlines and temperature contours in the longitudinal central plane in the trussed fin-and-elliptical tube channels of the different geometric configurations of PCL structures with 92% and 98% porosity, at $\mathrm{Re}_{D_h} = 3000$.

For every enhanced case, the PCL structure with 92% porosity has bigger cross-section vertices than the other porosity and results in further evident blockage and manipulation of the airflow by the vertices and ligaments. So, this is why the wider cross-sectional area of a vertex can intensify the secondary flow vortices. It can be seen from these figures that before the separation saddle point of the elliptical tube, the boundary layer flow rolls up and the horseshoe vortices begin from the vicinity of the stagnation point in front of each vertex and extend further downstream. Downstream of each vertex, large flow separation appears; thus, a pair of counter-rotating streamwise vortices is present.

For all the enhanced cases studied, as the porosity decreases to 92%, the downstream temperature and average temperature on the fin surface is reduced. This occurs because the vortex intensity becomes significantly higher as the porosity decreases, hence leading to an increase of the heat transfer rate. Temperature contours for the case BCCZ lattice structure indicate that the HTP in the downstream region is improved and the airflow temperature decreases rapidly in the main flow direction. This is predominantly due to the wider vertex cross-sectional area and narrower tortuous fluid flow path compared to the other cases.

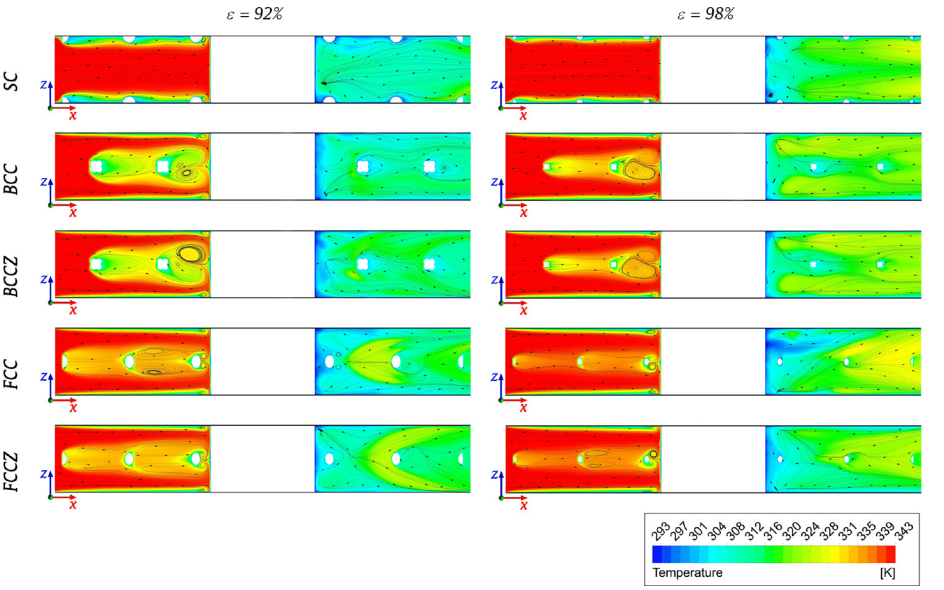

Figure 11.
Velocity streamlines and temperature contours in longitudinal central plane at $y = P_t/2$, $Re_{D_h} = 3000$

The contour plots of the velocity field for the cases PCL structures, with 92% and 98% porosity, on the *xy*-plane at the middle horizontal plane between two fins, are depicted in Figures 12 and 13, respectively, at $Re_{D_h} = 3000$. It is noteworthy that for a trussed fin equipped with PCL structures, because the airflow is constantly interrupted close to the surface, hence the flow structures near the trussed fin surface are significantly different from those for a plain fin surface. In the design of FTHXs, it is well realized that the heat transfer rate in wake zones downstream the tubes is relatively weak due to recirculation, and the airflow in this region is barely mixed with the main flow. Thus, the wake region should be decreased as far as possible. The PCL structures create tortuous flow-paths to promote mixing and disturbance of the fluid flow in the finned elliptical tube channel.

The local distributions of the velocity around the elliptical tubes and PCL structures are illustrated clearly in Figures 12 and 13, and these provide qualitative aspects of the parametric design of the PCL structures. Indeed, this gives a perception of the THP of a trussed FETHX for a detailed analysis and qualitative evaluation of the influence of the cell topology and porosity of the PCL structures. It can be observed from these velocity distributions that the airflow passes around the elliptical tubes and accelerates downstream.

When the PCL structures are used as a novel flow manipulator with the appropriate cell topology and porosity, the scale of the wake region behind the tube is highly constrained. The airflow which goes through the lattice of ligaments performs like local jet-flows with a random discharging direction that can aid the formation of strong vortices in the wake region. As observed from these distributions, it is evident that in the PCL structures with 92% porosity, the velocity of the airflow increases due to the formation and evolution of the secondary flow vortices and the blockage of the airflow by the ligaments. On the other hand, it is clear that the size of the wake region behind the elliptical tube for the case of PCL structures with 92% porosity is considerably smaller than that for the case with 98% porosity at the same Reynolds number. Consequently, the highly turbulent airflow mixing in

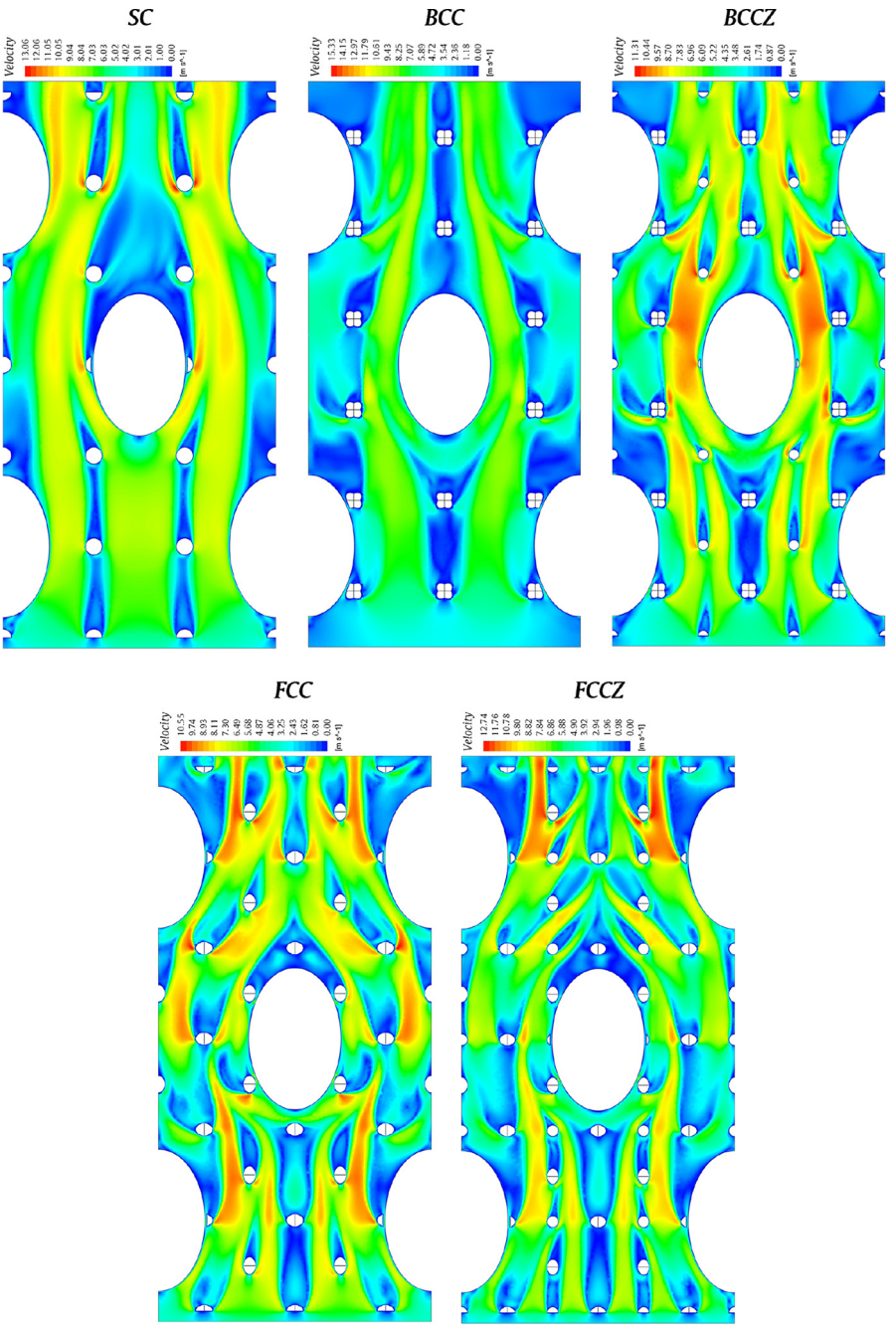

Figure 12.
Local distribution of the velocity (in the middle *xy*-plane) for PCLs at $\varepsilon = 92\%$, $\mathrm{Re}_{D_h} = 3000$

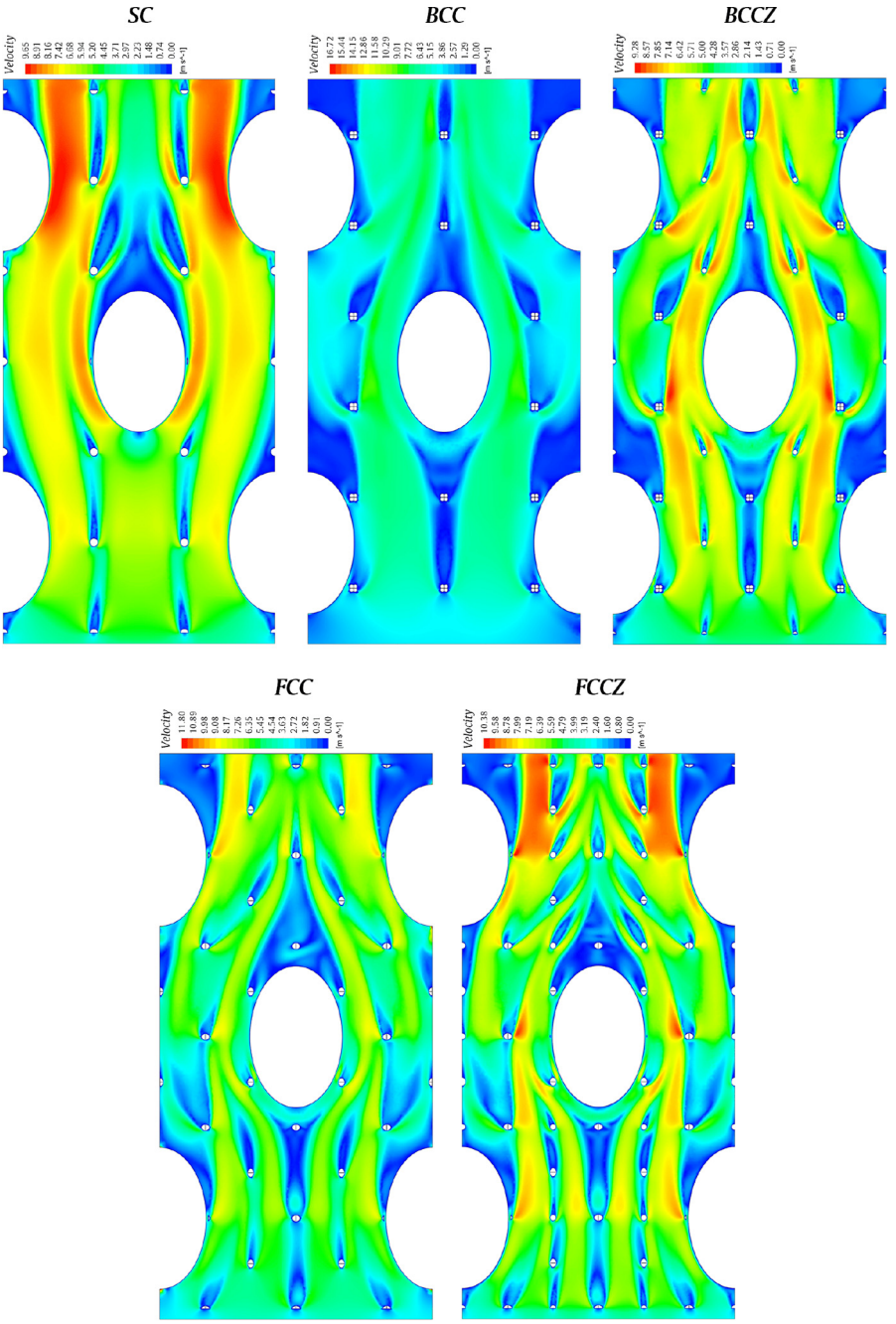

Figure 13.
Local distribution of the velocity (in the middle *xy*-plane) for PCLs at $\varepsilon = 98\%$, $\mathrm{Re}_{D_h} = 3000$

the case of PCL structures with 92% porosity gives a higher overall heat transfer performance.

Figures 14 and 15 display the contour plots of the local Nusselt number *Nu* on the trussed fin surfaces for the enhanced PCL structures with 92% and 98% porosity at $Re_{D_h} = 3000$. In every enhanced case, it is obvious that the maximum value of the Nusselt number occurs at the leading edge of the plain fin and then diminishes gradually in the streamwise direction because of the thermal boundary layer effect. The regions of high Nusselt number are observable not only around vertices but also along the downstream of each ligament. The former is owing to the existence of a horseshoe vortex, while the latter outcomes from the flow reattachment and recirculation of the wakes of the ligaments.

Figures 14 and 15 demonstrate the local Nusselt number *Nu* distributions on the PCL ligaments for the five enhanced cases. It is well observed that the local heat transfer on the upstream surface of the ligament is higher than that on the downstream surface of the ligament for all the PCL structures, which is dominated by the high-momentum impingement airflow and low-momentum secondary flows, respectively. However, compared to all the enhanced cases, the BCCZ and FCCZ lattice structures reveal a remarkable higher local Nusselt number *Nu* on the upstream surface of the ligaments, because these structures have vertices with more overlapping ligaments on the fin surface, and therefore, further augmentation of the heat-exchange between the core ligaments and the main flow occurs.

The effect of porosity value ε and cell topology shown in these figures for the BCCZ lattice structure with 92% porosity (owing to the widest projected surface area facing the airflow which causes the highest vortex intensity), visualize that the wake regions behind the elliptical tubes become smaller and the mainstream flow at high temperature is directed towards the tubes leading to better heat transfer performance.

4.3 Heat transfer and fluid flow performance of new elliptical tube-banks

To investigate the influence of the cell topology and porosity of the PCL structures on the thermal-flow field characterization for novel trussed FETHXs, a comparative study for FETHXs with PCL core and without PCL core was accomplished. It is worth mentioning that the FETHX without PCL core will be referred to as a "baseline" (un-enhanced) case and the FETHX with PCL core will be referred to as "enhanced" cases. Figure 16 depicts the effect of the porosity ε on the variation of the average Nusselt number *Nu* versus Reynolds number Re_{D_h} for five diverse topologies of PCL structure, i.e. SC, BCC, BCCZ, FCC and FCCZ. One may observe from Figure 16 that the average Nusselt number *Nu* for both the baseline case and the five enhanced cases increases with increasing Reynolds number. As expected, the average Nusselt number *Nu* of the trussed FETHXs with PCL core is larger than that of the baseline case at various Reynolds numbers.

The general trend for all the enhanced cases is that a reduction in porosity to 92%, which is associated with an increase in the interfacial surface area, leads to increases in the average Nusselt number *Nu*. It means that increasing the ligament diameter has a substantial effect on the heat transfer performance on the trussed FETHXs.

According to Figure 16, the average Nusselt numbers *Nu* in the BCCZ and FCCZ lattice structures, are mainly caused by better disturbance of airflow. The values are higher than for the other enhanced cases. Concerning the porosity effectiveness evaluation, the BCCZ lattice structure with 92% porosity possesses the highest average Nusselt number *Nu* as compared to that of the other PCL structures.

The influence of the porosity ε on the relation between the friction factor f and the Reynolds number Re_{D_h} for the five diverse PCL structures studied in this investigation is

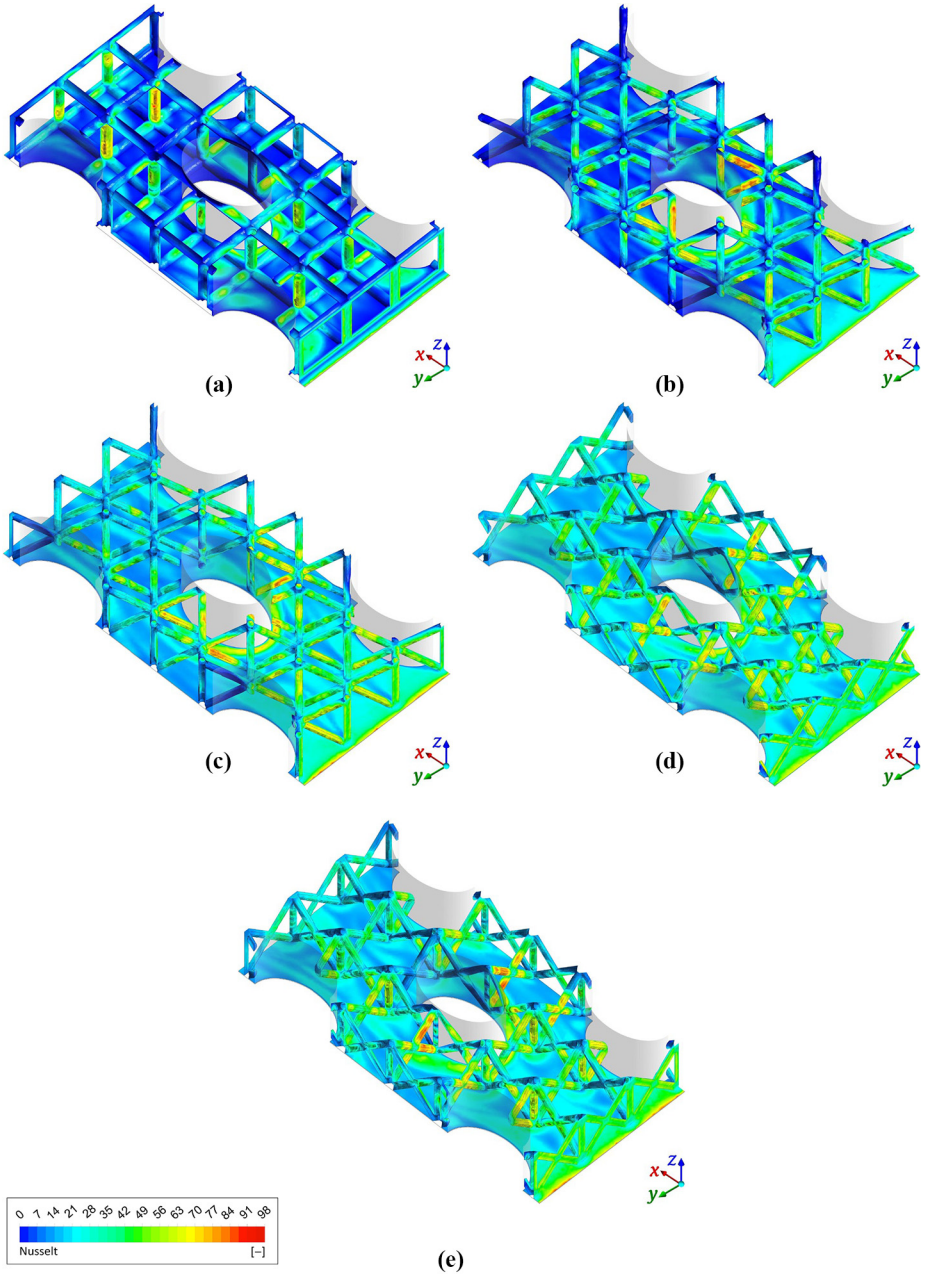

Figure 14.
Distribution of local Nusselt number on the ligaments and inner surface of the lower fin, for PCLs at $\varepsilon = 92\%$, $\mathrm{Re}_{D_h} = 3000$

Notes: (a) SC; (b) BCC; (c) BCCZ; (d) FCC; (e) FCCZ

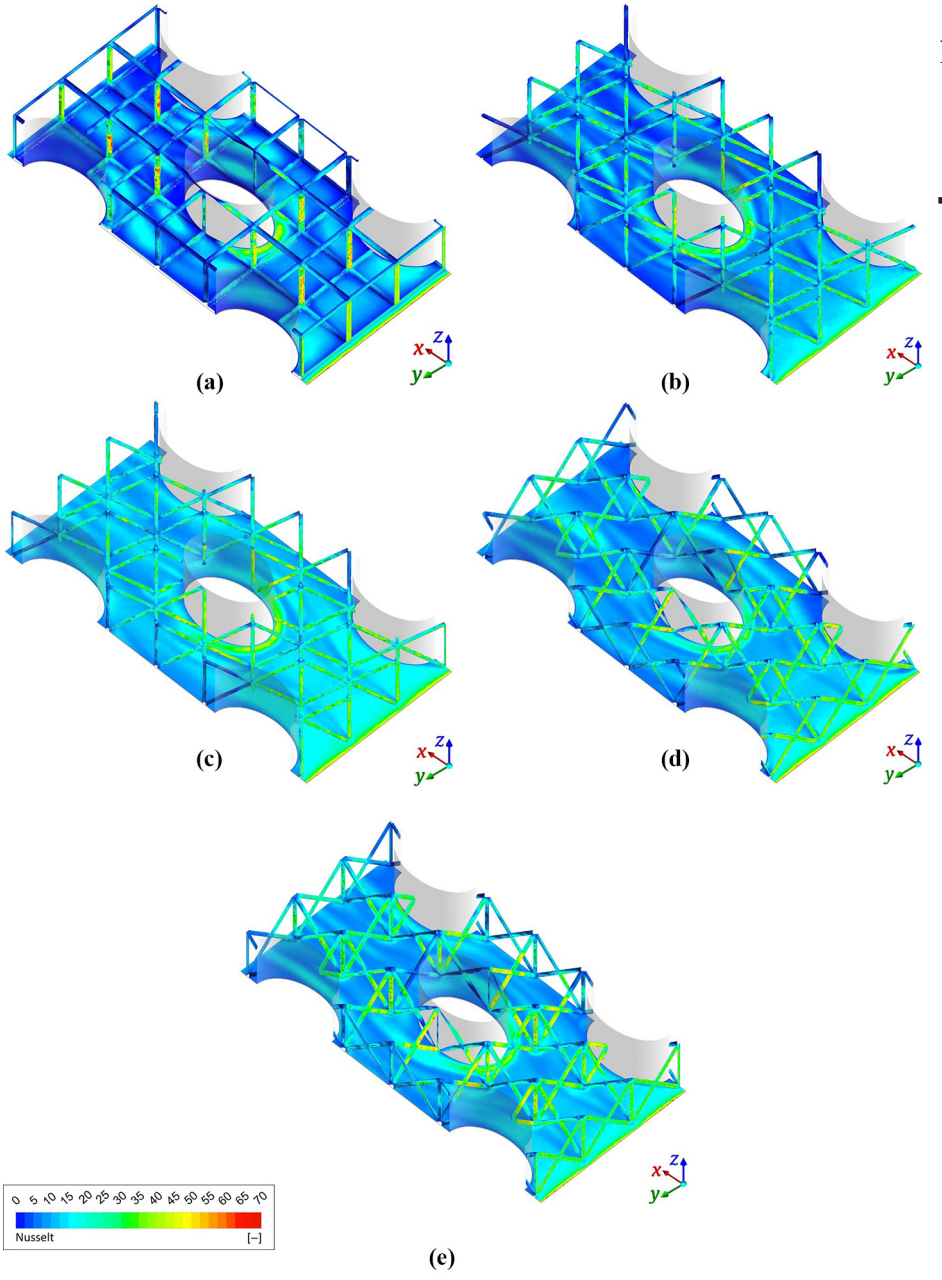

Notes: (a) SC; (b) BCC; (c) BCCZ; (d) FCC; (e) FCCZ

Figure 15.
Distribution of local Nusselt number on the ligaments and inner surface of the lower fin, for PCLs at $\varepsilon = 98\%$, $\mathrm{Re}_{D_h} = 3000$

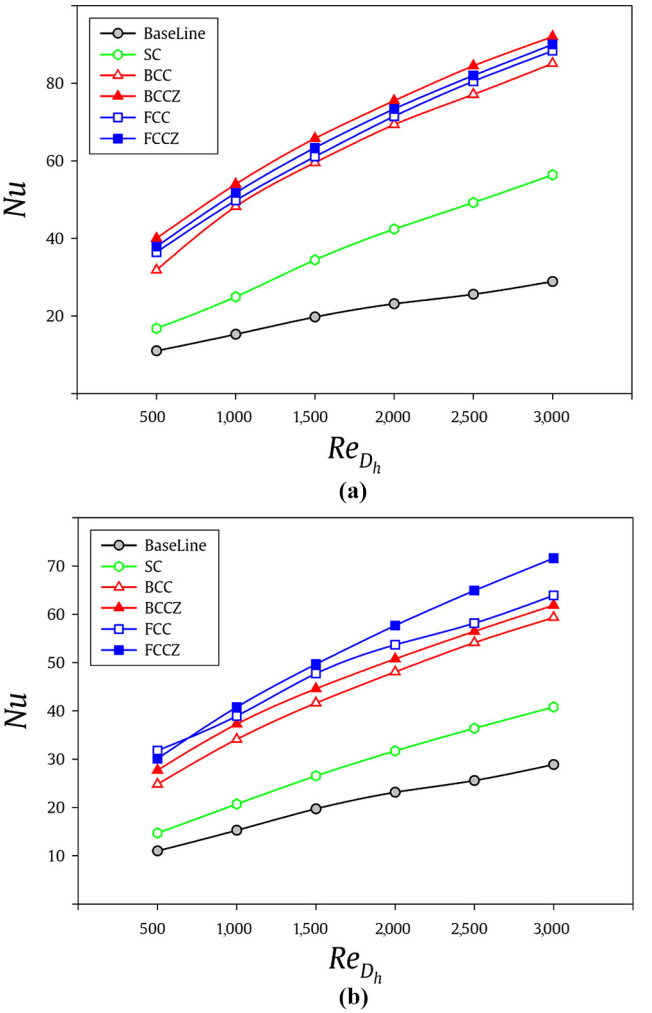

Figure 16.
Influence of porosity value ε of PCL structures on average Nusselt number Nu

Notes: (a) $\varepsilon = 92\%$; (b) $\varepsilon = 98\%$

illustrated in Figure 17. The friction factor f represents the attributes desired to specify pressure drop characteristics for different geometry conditions and given airflow rate. As it is observed the f decreases with an increase of Re_{D_h} for all the cases considered. In addition, one can clearly see that when the Reynolds number Re_{D_h} is raised within the considered range, the variation in the drag coefficient is reduced and above a certain Reynolds number it becomes nearly constant. As is evident, the variation of the porosity for every enhanced case can establish perceptible difference in the friction factor f, and as expected, the friction factor f is inversely proportional to the porosity. The simulation results have implied that with the high porosity 98%, the friction factor f appreciably declines, indicating an increasing the free area available for airflow in the PCL structure with higher porosity. As

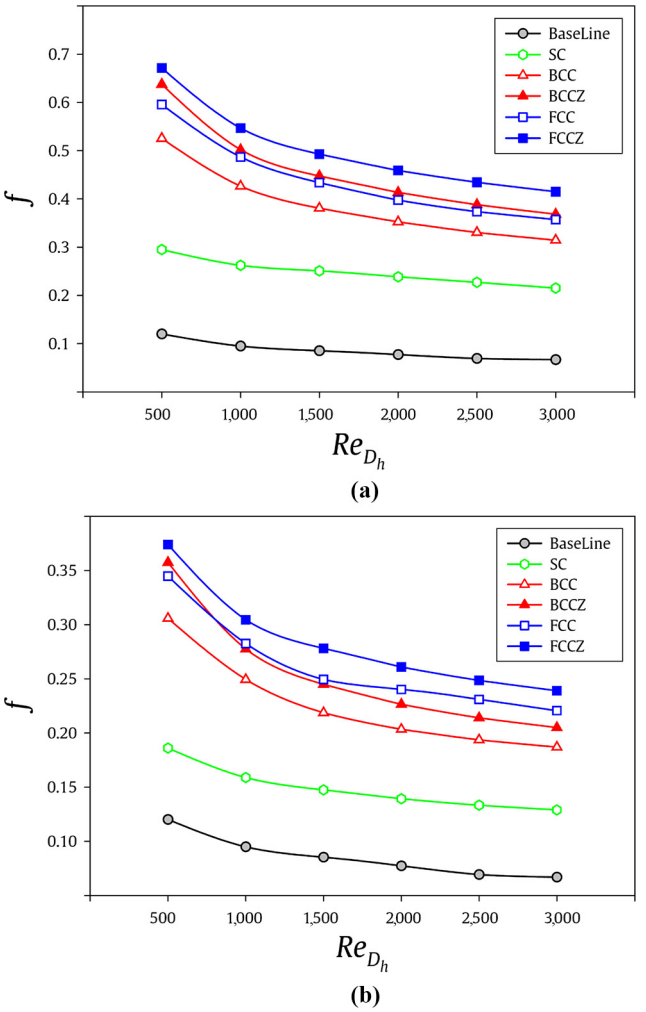

Notes: (a) $\varepsilon = 92\%$; (b) $\varepsilon = 98\%$

Figure 17.
Influence of porosity value ε of PCL structures on friction factor f

shown in Figure 17, the SC and BCC lattice structures have the least friction factor f owing to the less channel blockage together with a smaller surface drag than that of the other PCL structures.

4.4 Thermal-hydraulic performance benchmarks

4.4.1 Field synergy performance. From a survey of related literature about the concept of FSP, it is widely approved that the field synergy number can serve as the appropriate indicator for FSP, i.e. which physically is an indication of the degree of synergy between velocity and temperature gradient fields in the entire domain. Hence, in this section, the

influence of the porosity on the heat transfer enhancement for FETHX with high-porosity PCL structures is analyzed according to the field synergy principle.

Figure 18 depicts the variation of the average field synergy number *Fc* of all the enhanced cases versus the Reynolds number Re_{D_h} for the two values of the porosity ε. From this figure, the FETHX with PCL core has the highest average field synergy number *Fc* at the same Reynolds number, while the FETHX without PCL core has the lowest average field synergy number *Fc*. These results explain the fact that the FETHX with PCL structure reveals a more significant heat transfer performance.

One may observe from Figure 18 that the average field synergy number *Fc* declines slightly with increasing Reynolds number Re_{D_h} for all studied cases, because increasing the

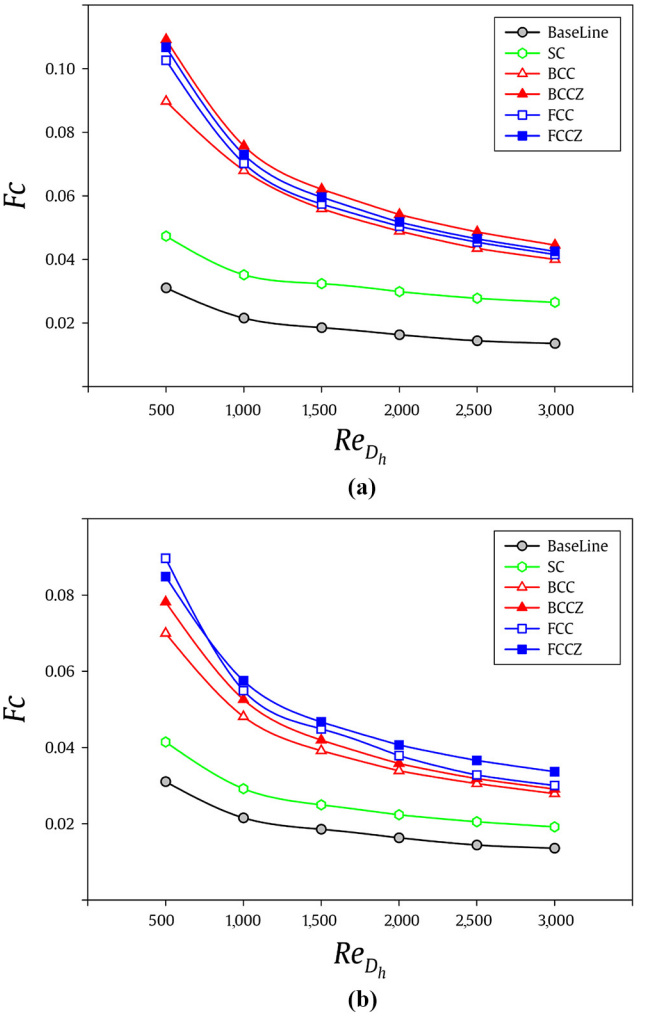

Figure 18.
Influence of porosity value ε of PCL structures on average field synergy number *Fc*

Notes: (a) $\varepsilon = 92\%$; (b) $\varepsilon = 98\%$

airflow velocity cannot cover thoroughly the increase in heat transfer coefficient, according to the *Fc* definition. From the standpoint of porosity effectiveness evaluation, the BCCZ lattice structure with 92% porosity possesses the highest average field synergy number *Fc* compared to the other PCL structures.

4.4.2 Performance evaluation criterion. Thermal-hydraulic aspects of CHX design have created numerous challenges for designers. Hereupon, continuous effective efforts have been made to improve the THP of CHXs in all thermal application fields.

As is well-known, the heat transfer and flow characteristics of CHXs, e.g. FTHXs in terms of the Nusselt number and the friction factor, are used to perform the THP evaluation between geometrically similar CHXs. Generally, the augmentation of the Nusselt number results in an increased heat transfer rate, and this will be associated with a reduction of thermodynamic cost. On the other hand, reduced pumping power due to dropping friction factor leads to a lower cost of a heat exchanger operation.

Based on the existing literature survey on the THP studies of FTHXs, it is found that the improvement in the thermal performance by using enhancement passive techniques is usually associated with an increase in the pressure drop penalty, which induces a higher pumping cost. Therefore, the optimum design of FTHXs is very complex, as it requires precise and extensive analysis of heat transfer rate and pressure drop simultaneously. Accordingly, any novel enhancement methods developed into the CHX, e.g. FTHX should be a balanced trade-off between the benefits of heat transfer coefficient and the higher pumping cost due to the raised frictional losses.

Two performance evaluation criteria were employed in this section of the study to assess the overall THP of the trussed FETHX with PCL structures with different high-porosities of 92% and 98%, namely, *modified flow area GF* (i.e. $j/f^{1/3}$ versus Re_{D_h}) and *core volume GF* (i.e. *Z* versus *E*). The modified flow area GF indicates essentially the direct analogy of the $j/f^{1/3}$ ratio as a function of Reynolds number Re_{D_h} for the purpose of identification of the extended surface needing the minimal frontal area for a constant pressure loss penalty. The influence of the porosity ε on the flow modified flow area GF at different Reynolds numbers for the five diverse PCL structures is shown in Figure 19. It is observed that the ratio of $j/f^{1/3}$ tends to decrease with the increase of Reynolds number. For the enhanced cases PCL structures studied, the ratio of PEC index $j/f^{1/3}$ for BCCZ and FCCZ lattice structure with 92% and 98% porosity, respectively, is higher than that of the other enhanced cases.

The flow area GF method does not alone serve as a definite effective assessment tool; because in addition to the effect of pressure drop, the entire volume of CHX must be considered. Accordingly, another PEC of the CHX is assessed and determined by the core volume GF method, which compares the isothermal heat transport per unit core volume (*Z*) to the pumping power required per unit core volume (*E*).

In the present study, from the standpoint of the trussed FETHX volume required, configuration geometries with larger values of *Z* will need less core volume for a given air-side heat transfer capacity. Figure 20 depicts the core volume GF for different enhanced cases PCL structures with two values of the porosity ε. The BCCZ lattice structure case with 92% porosity has a slightly higher value than other enhanced cases. On the other hand, Figure 20(b) shows that the FCCZ lattice structure case with 98% porosity transfers the highest heat flux per unit volume for the same pumping power per unit volume. Considering Figures 19 and 20, because of PEC, one can see that if the porosity is decreased to 92%, which in turn increases the diameter of the ligaments, will yield a more desirable surface based on these performance metrics.

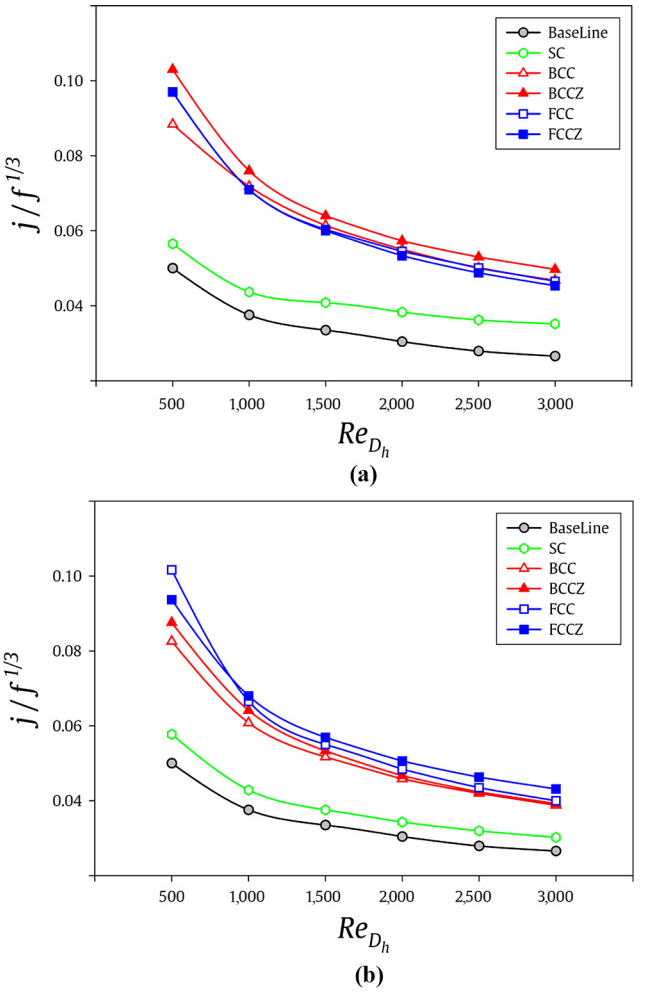

Figure 19.
Modified flow area goodness factor criterion for PCLs

Notes: (a) $\varepsilon = 92\%$; (b) $\varepsilon = 98\%$

4.5 Pec comparison: influence of enhanced fin patterns

As is well-known, the heat transfer performance of FTHXs is highly dependent on the structure of fins because the dominant thermal resistance is generally on the air-side. The purpose of next generation CHXs is to increase the THP due to combined enhancement techniques and thereby improve the energy-efficiency. Hence, currently, the utilization of enhanced fin patterns is very appropriate in advanced FTHXs.

To reveal the importance of this issue, a number of enhanced FTHXs were compared, namely – louvered FTHX (Okbaz *et al.*, 2020), wavy FTHX (Okbaz *et al.*, 2020), wavy FETHX with rectangular trapezoidal winglet (RTW) vortex generators at attack angle 60° (Lotfi *et al.*, 2014a), FETHX with upward triangular dimple (UwTD) turbulators (Lotfi and Sundén, 2020b), and trussed FETHX with BCCZ lattice structure at 92% porosity

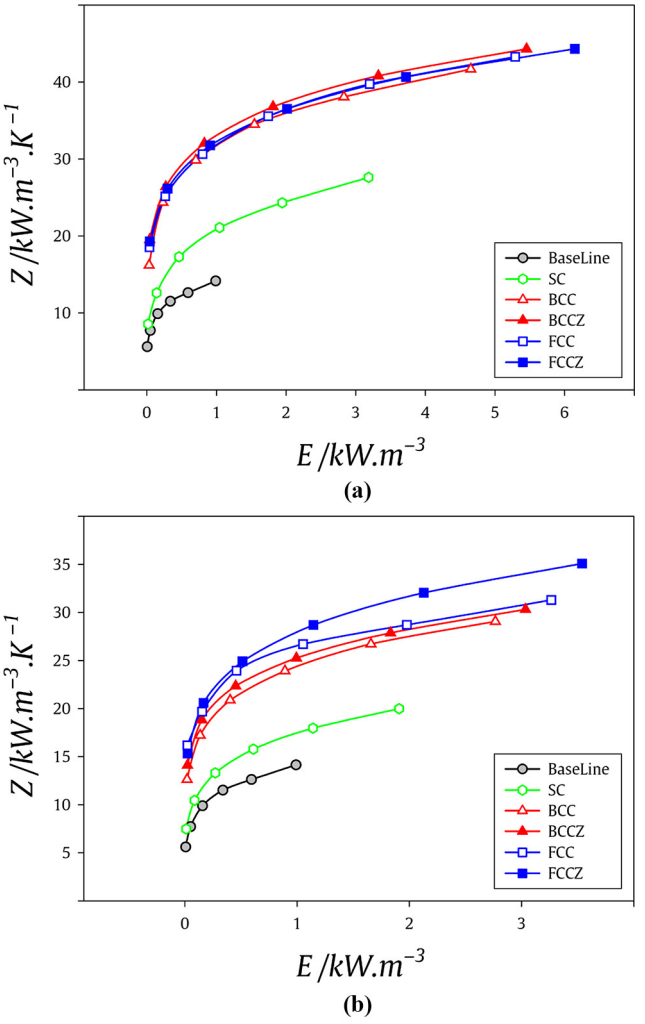

Notes: (a) $\varepsilon = 92\%$; (b) $\varepsilon = 98\%$

Figure 20.
Core volume goodness factor criterion for PCLs

(i.e. present study), by two key performance evaluation criteria, i.e. modified flow area GF and core volume GF. The results of these comparisons are presented in Figure 21.

It can be seen that the trussed FETHX with BCCZ lattice structure at $\varepsilon = 92\%$ provides a better flow modified flow area GF than the other enhanced cases. An overview of Figure 21(b) reveals that the trussed FETHX with BCCZ lattice structure at $\varepsilon = 92\%$ and then wavy FETHX with RTW vortex generators at $\alpha = 60°$ have the higher core volume GF than the other enhanced cases.

An important point should be noted, by changing the essential design parameters such as the longitudinal and transverse tube pitch and also specifically the tube diameter and fin

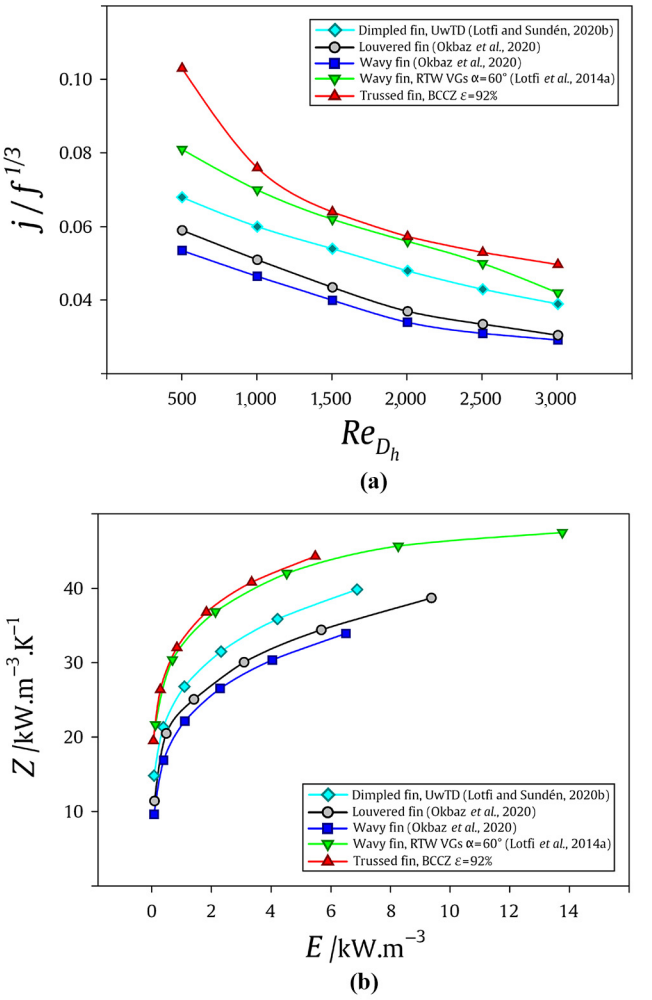

Figure 21.
PEC comparison of several enhanced FTHXs

Notes: (a) $j/f^{1/3}$ *vs.*$_{D_h}$; (b) Z *vs.* E

pitch, etc., effectiveness of the flow manipulators and turbulators on the THP can be different and thus the comparison of the results will also be changed.

5. Concluding remarks

The thermal-hydraulic studies reveal clearly that the capabilities of CMs are extremely evident for advanced thermal energy transfer devices such as compact heat exchangers. Hence, a novel trussed finned elliptical tube heat exchanger aimed at representing the potential benefits of applying high-porosity periodic cellular lattice materials is proposed in this paper.

In the present investigation, three-dimensional CFD numerical simulations were conducted to clarify and explore the influences of periodic cellular lattice fin configuration

geometry characteristics and high-porosity values on the thermal-hydraulic performance of the novel trussed fin-and-elliptical tube heat exchanger. The highlights of conclusions drawn in this investigation are summarized as follows:

- The local dominant flow patterns and features in the trussed FETHX consisting of the lattice structures were identified. Multiform and complex secondary flow vortex structures around the vertices of the PCL include the horseshoe and arch-shaped vortices, which formed upstream and downstream of the vertices, respectively, and the flow separation on the ligament surfaces leading to a substantial increase in the heat transfer performance.
- Investigating the influence of morphological parameters–such as lattice structure topology (SC, BCC, BCCZ, FCC and FCCZ lattice structures) and porosity value (ε = 92% – 98%)–on the thermal-hydraulic characteristics has led to a deeper understanding of the interaction between fluid flow and PCL structure in trussed FETHX.
- Benchmark analyses of the thermal-hydraulic performance such as "field synergy performance" (i.e. synergy number) and "performance evaluation criterion" (i.e. flow area goodness factor and core volume goodness factor) have been carried out to study the heat transfer and pressure drop characteristics in trussed FETHX utilized PCL structures.
- Based on the predicted friction factor f of this study, it is revealed that with a high porosity value by 98%, the pressure drop appreciably declines, indicating an increasing free area available for airflow in the PCL structure with higher porosity.
- A cell topology investigation of the PCL structures using the performance assessment benchmarks showed that BCCZ and FCCZ lattice structure with 92% and 98% porosity, respectively, has better thermal-hydraulic performance enhancement compared to the other PCL structures.
- The computational results showed that the rate of FSP and PEC indices of the PCL structures decreases as the porosity value increases. Thereby, it has been demonstrated that if the high-porosity of all PCL structures decreases to 92%–which in turn increases the diameter of the ligaments, the increment in the heat transfer surface area density–provides the best thermal-hydraulic performance.

It is worth mentioning that despite the many limitations on the production of CMs, noteworthy opportunities exist to maximize the thermal-hydraulic performance of advanced compact heat exchangers with periodic cellular lattice structures via varying the lattice cell morphological and type of metallic alloy used

References

Almogbel, M. and Bejan, A. (2000), "Cylindrical trees of pin fins", *International Journal of Heat and Mass Transfer*, Vol. 43 No. 23, pp. 4285-4297.

ANSYS CFX (2018), *ANSYS CFX-Solver Theory Guide: Release 19*, ANSYS, Canonsburg, PA, Vol. 2.

ANSYS ICEM (2018), *ANSYS ICEM CFD User's Manual: Release 19*, ANSYS, Canonsburg, PA, Vol. 2.

Arasteh, H., Salimpour, M.R. and Tavakoli, M.R. (2019), "Optimal distribution of metal foam inserts in a double-pipe heat exchanger", *International Journal of Numerical Methods for Heat and Fluid Flow*, Vol. 29 No. 4, pp. 1322-3142.

Ashby, M.F., Evans, A., Fleck, N.A., Gibson, L.J., Hutchinson, J.W. and Wadley, H.N.G. (2000), *Metal Foams: A Design Guide*, Butterworth-Heinemann, Oxford.

Bear, J. (1972), *Dynamics of Fluids in Porous Media*, American Elsevier Publishing, New York, NY.

Bejan, A. (1997), "Constructal-theory network of conducting paths for cooling a heat generating volume", *International Journal of Heat and Mass Transfer*, Vol. 40 No. 4, pp. 799-816.

Bracconi, M., Ambrosetti, M., Okafor, O., Sans, V., Zhang, X., Ou, X., Da Fonte, C.P., Fan, X., Maestri, M., Groppi, G. and Tronconi, E. (2019), "Investigation of pressure drop in 3D replicated open-cell foams: coupling CFD with experimental data on additively manufactured foams", *Chemical Engineering Journal*, Vol. 377, p. 120123.

Buonomo, B., di Pasqua, A., Manca, O. and Nardini, S. (2020), "Evaluation of thermal and fluid dynamic performance parameters in aluminum foam compact heat exchangers", *Applied Thermal Engineering*, Vol. 176, p. 115456.

Calmidi, V.V. and Mahajan, R.L. (1999), "The effective thermal conductivity of high porosity fibrous metal foams", *Journal of Heat Transfer*, Vol. 121 No. 2, pp. 466-471.

Chai, L. and Tassou, S. (2018), "A review of airside heat transfer augmentation with vortex generators on heat transfer surface", *Energies*, Vol. 11 No. 10, p. 2737.

Chen, K., Guo, L. and Wang, H. (2020), "A review on thermal application of metal foam", *Science China Technological Sciences*, Vol. 63 No. 12, pp. 2469-2490.

Cheng, Y.P., Lee, T.S. and Low, H.T. (2009), "Numerical prediction of periodically developed fluid flow and heat transfer characteristics in the sinusoid wavy fin-and-tube heat exchange", *International Journal of Numerical Methods for Heat and Fluid Flow*, Vol. 19 No. 6, pp. 728-744.

Chennu, R. and Paturu, P. (2011), "Development of heat transfer coefficient and friction factor correlations for offset fins using CFD", *International Journal of Numerical Methods for Heat and Fluid Flow*, Vol. 21 No. 8, pp. 935-951.

Chu, W.X., Sheu, W.J., Hsu, C.C. and Wang, C.C. (2020), "Airside performance of sinusoidal wavy fin-and-tube heat exchangers subject to large-diameter tubes with round or oval configuration", *Applied Thermal Engineering*, Vol. 164, p. 114469.

Collins, R.E. (1976), *Flow of Fluids through Porous Materials*, PennWell Publishing, Tulsa, Oklahoma.

Cunsolo, S., Iasiello, M., Oliviero, M., Bianco, N., Chiu, W.K.S. and Naso, V. (2016), "Lord Kelvin and Weaire–Phelan foam models: heat transfer and pressure drop", *Journal of Heat Transfer*, Vol. 138 No. 2, p. 22601.

DeJong, N.C. and Jacobi, A.M. (1999), "Local flow and heat transfer behavior in convex-louver fin arrays", *Journal of Heat Transfer*, Vol. 121 No. 1, pp. 136-141.

Dietrich, B. (2012), "Pressure drop correlation for ceramic and metal sponges", *Chemical Engineering Science*, Vol. 74, pp. 192-199.

Dietrich, B., Schabel, W., Kind, M. and Martin, H. (2009), "Pressure drop measurements of ceramic sponges – determining the hydraulic diameter", *Chemical Engineering Science*, Vol. 64 No. 16, pp. 3633-3640.

Dogan, S., Darici, S. and Ozgoren, M. (2019), "Numerical comparison of thermal and hydraulic performances for heat exchangers having circular and elliptic cross-section", *International Journal of Heat and Mass Transfer*, Vol. 145, p. 118731.

Du Plessis, P., Montillet, A., Comiti, J. and Legrand, J. (1994), "Pressure drop prediction for flow through high porosity metallic foams", *Chemical Engineering Science*, Vol. 49 No. 21, pp. 3545-3553.

Du Plessis, A., Razavi, S.M.J., Benedetti, M., Murchio, S., Leary, M., Watson, M., Bhate, D. and Berto, F. (2022), "Properties and applications of additively manufactured metallic cellular materials: a review", *Progress in Materials Science*, Vol. 125, p. 100918.

Dukhan, N. and Hmad, A.A. (2022), "Thermal management of fuel-cell stacks using air flow in open-cell metal foam", *International Journal of Thermal Sciences*, Vol. 172, p. 107370.

Ebisu, T. (1999), "Development of new concept air-cooled heat exchanger for energy conservation of air-conditioning machine", in Kakaç, S., Bergles, A.E., Mayinger, F. and Yüncü, H. (Eds) *Heat Transfer Enhancement of Heat Exchangers*, Springer, Dordrecht, pp. 601-620.

Edouard, D., Lacroix, M., Huu, C.P. and Luck, F. (2008), "Pressure drop modeling on solid foam: state-of-the art correlation", *Chemical Engineering Journal*, Vol. 144 No. 2, pp. 299-311.

Ettrich, J. (2014), *Fluid Flow and Heat Transfer in Cellular Solids*, KIT Scientific Publishing, Karlsruhe.

Fu, Y., Wen, J. and Zhang, C. (2017), "An experimental investigation on heat transfer enhancement of sprayed wire-mesh heat exchangers", *International Journal of Heat and Mass Transfer*, Vol. 112, pp. 699-708.

Fugmann, H., Laurenz, E. and Schnabel, L. (2017), "Wire structure heat exchangers – new designs for efficient heat transfer", *Energies*, Vol. 10 No. 9, p. 1341.

Fugmann, H., Martens, S., Balzer, R., Brenner, M., Schnabel, L. and Mehring, C. (2020), "Performance evaluation of wire cloth micro heat exchangers", *Energies*, Vol. 13 No. 3, p. 715.

Fujii, M., Seshimo, Y. and Yamanaka, G. (1988), "Heat transfer and pressure drop of perforated surface heat exchanger with passage enlargement and contraction", *International Journal of Heat and Mass Transfer*, Vol. 31 No. 1, pp. 135-142.

Gao, L. and Sun, Y.G. (2014), "Fluid flow and heat transfer characteristics of composite lattice core sandwich structures", *Journal of Thermophysics and Heat Transfer*, Vol. 28 No. 2, pp. 258-269.

Gholami, A., Wahid, M.A. and Mohammed, H.A. (2017), "Thermal–hydraulic performance of fin-and-oval tube compact heat exchangers with innovative design of corrugated fin patterns", *International Journal of Heat and Mass Transfer*, Vol. 106, pp. 573-592.

Gibson, L.J. and Ashby, M.F. (1999), *Cellular Solids: Structure and Properties*, Cambridge University Press, Cambridge.

Guo, Z.Y., Li, D.Y. and Wang, B.X. (1998), "A novel concept for convective heat transfer enhancement", *International Journal of Heat and Mass Transfer*, Vol. 41 No. 14, pp. 2221-2225.

Guo, Z.Y., Tao, W.Q. and Shah, R.K. (2005), "The field synergy (coordination) principle and its applications in enhancing single phase convective heat transfer", *International Journal of Heat and Mass Transfer*, Vol. 48 No. 9, pp. 1797-1807.

Guo, J., Xu, M. and Cheng, L. (2011), "Numerical investigations of curved square channel from the viewpoint of field synergy principle", *International Journal of Heat and Mass Transfer*, Vol. 54 Nos 17/18, pp. 4148-4151.

Hall, M.J. and Hiatt, J.P. (1996), "Measurements of pore scale flows within and exiting ceramic foams", *Experiments in Fluids*, Vol. 20 No. 6, pp. 433-440.

Hammetter, C.I., Rinaldi, R.G. and Zok, F.W. (2013), "Pyramidal lattice structures for high strength and energy absorption", *Journal of Applied Mechanics*, Vol. 80 No. 4, p. 41015.

Han, X.-H., Wang, Q., Park, Y.-G., T'Joen, C., Sommers, A. and Jacobi, A. (2012), "A review of metal foam and metal matrix composites for heat exchangers and heat sinks", *Heat Transfer Engineering*, Vol. 33 No. 12, pp. 991-1009.

Hasan, A. and Sirén, K. (2004), "Performance investigation of plain circular and oval tube evaporatively cooled heat exchangers", *Applied Thermal Engineering*, Vol. 24 Nos 5/6, pp. 777-790.

He, Y.L. and Tao, W.Q. (2014), "Chapter three - convective heat transfer enhancement: mechanisms, techniques, and performance evaluation", *Advances in Heat Transfer*, Vol. 46, pp. 87-186.

Hooman, K., Tamayol, A. and Malayeri, M.R. (2012), "Impact of particulate deposition on the thermohydraulic performance of metal foam heat exchangers: a simplified theoretical model", *Journal of Heat Transfer*, Vol. 134 No. 9, p. 92601.

Huisseune, H., De Schampheleire, S., Ameel, B. and De Paepe, M. (2015), "Comparison of metal foam heat exchangers to a finned heat exchanger for low Reynolds number applications", *International Journal of Heat and Mass Transfer*, Vol. 89, pp. 1-9.

Huu, T.T., Lacroix, M., Pham Huu, C., Schweich, D. and Edouard, D. (2009), "Towards a more realistic modeling of solid foam: use of the pentagonal dodecahedron geometry", *Chemical Engineering Science*, Vol. 64 No. 24, pp. 5131-5142.

Kays, W.M. and London, A.L. (1950), "Heat transfer and flow friction characteristics of some compact heat exchanger surfaces", *Transactions of the ASME*, Vol. 72, pp. 1075-1097.

Kemerli, U. and Kahveci, K. (2020), "Conjugate forced convective heat transfer in a sandwich panel with a Kagome truss core: the effects of strut length and diameter", *Applied Thermal Engineering*, Vol. 167, p. 114794.

Khaled, A.R.A. (2007), "Heat transfer enhancement in hairy fin systems", *Applied Thermal Engineering*, Vol. 27 No. 1, pp. 250-257.

Kim, T., Hodson, H.P. and Lu, T.J. (2005), "Contribution of vortex structures and flow separation to local and overall pressure and heat transfer characteristics in an ultra-lightweight lattice material", *International Journal of Heat and Mass Transfer*, Vol. 48 Nos 19/20, pp. 4243-4264.

Kotresha, B. and Gnanasekaran, N. (2020), "Numerical simulations of fluid flow and heat transfer through aluminum and copper metal foam heat exchanger – a comparative study", *Heat Transfer Engineering*, Vol. 41 Nos 6/7, pp. 637-649.

Kouidri, A. and Madani, B. (2017), "Thermal and hydrodynamic performance of flow boiling through a heat exchanger filled with various metallic foam samples", *Chemical Engineering and Processing: Process Intensification*, Vol. 121, pp. 162-169.

Krishnan, S.G., Bodla, K.K., Weibel, J.A. and Garimella, S.V. (2014), "Numerical investigation of fluid flow and heat transfer in periodic porous lattice-flame materials", *15th international heat transfer conference*, *Kyoto*, 10-15 August, pp. 6651-6665.

Li, Y., Gong, L., Ding, B., Xu, M. and Joshi, Y. (2021a), "Thermal management of power electronics with liquid cooled metal foam heat sink", *International Journal of Thermal Sciences*, Vol. 163, p. 106796.

Li, Y., Gong, L., Xu, M. and Joshi, Y. (2021b), "A review of thermo-hydraulic performance of metal foam and its application as heat sinks for electronics cooling", *Journal of Electronic Packaging*, Vol. 143 No. 3, p. 30801.

Li, S.F., Liu, Z.H. and Wang, X.J. (2019), "A comprehensive review on positive cold energy storage technologies and applications in air conditioning with phase change materials", *Applied Energy*, Vol. 255, p. 113667.

Li, X.Y., Mu, Y.T., Li, Z.H. and Tao, W.Q. (2020), "Numerical study on the heat transfer and pressure drop characteristics of fin-and-tube surface with four round-convex strips around each tube", *International Journal of Heat and Mass Transfer*, Vol. 158, p. 120034.

Liang, D., He, G., Chen, W., Chen, Y. and Chyu, M.K. (2022), "Fluid flow and heat transfer performance for micro-lattice structures fabricated by selective laser melting", *International Journal of Thermal Sciences*, Vol. 172, p. 107312.

Lotfi, B. and Sundén, B. (2020a), "Development of new finned tube heat exchanger: innovative tube-bank design and thermohydraulic performance", *Heat Transfer Engineering*, Vol. 41 No. 14, pp. 1209-1231.

Lotfi, B. and Sundén, B. (2020b), "Thermo-hydraulic performance enhancement of finned elliptical tube heat exchangers by utilizing innovative dimple turbulators", *Heat Transfer Engineering*, Vol. 41 No. 13, pp. 1117-1142.

Lotfi, B., Sundén, B. and Wang, Q.-W. (2016a), "3D fluid-structure interaction (FSI) simulation of new type vortex generators in smooth wavy fin-and-elliptical tube heat exchanger", *Engineering Computations*, Vol. 33 No. 8, pp. 2504-2529.

Lotfi, B., Sundén, B. and Wang, Q. (2016b), "An investigation of the thermo-hydraulic performance of the smooth wavy fin-and-elliptical tube heat exchangers utilizing new type vortex generators", *Applied Energy*, Vol. 162, pp. 1282-1302.

Lotfi, B., Zeng, M., Sundén, B. and Wang, Q. (2014a), "3D numerical investigation of flow and heat transfer characteristics in smooth wavy fin-and-elliptical tube heat exchangers using new type vortex generators", *Energy*, Vol. 73 No. 14, pp. 233-257.

Lotfi, B., Zeng, M., Sundén, B. and Wang, Q. (2014b), "Thermo-hydraulic characterization of the smooth wavy fin-and-elliptical tube heat exchangers using new type vortex generators", *Energy Procedia*, Vol. 61, pp. 2343-2346.

Lu, T.J., Stone, H.A. and Ashby, M.F. (1998), "Heat transfer in open-cell metal foams", *Acta Materialia*, Vol. 46 No. 10, pp. 3619-3635.

Mahjoob, S. and Vafai, K. (2008), "A synthesis of fluid and thermal transport models for metal foam heat exchangers", *International Journal of Heat and Mass Transfer*, Vol. 51 Nos 15/16, pp. 3701-3711.

Mangrulkar, C.K., Dhoble, A.S., Chamoli, S., Gupta, A. and Gawande, V.B. (2019), "Recent advancement in heat transfer and fluid flow characteristics in cross flow heat exchangers", *Renewable and Sustainable Energy Reviews*, Vol. 113, p. 109220.

Menter, F.R. (1994), "Two-equation eddy-viscosity turbulence models for engineering applications", *AIAA Journal*, Vol. 32 No. 8, pp. 1598-1605.

Moon, C., Kim, D., Bamorovat Abadi, G., Yoon, S.Y. and Kim, K.C. (2016), "Effect of ligament hollowness on heat transfer characteristics of open-cell metal foam", *International Journal of Heat and Mass Transfer*, Vol. 102, pp. 911-918.

Nawaz, K., Bock, J. and Jacobi, A.M. (2017), "Thermal-hydraulic performance of metal foam heat exchangers under dry operating conditions", *Applied Thermal Engineering*, Vol. 119, pp. 222-232.

Nield, D.A. and Bejan, A. (2017), *Convection in Porous Media*, Springer, New York, NY.

Okbaz, A., Pınarbaşı, A. and Olcay, A.B. (2020), "Experimental investigation of effect of different tube row-numbers, fin pitches and operating conditions on thermal and hydraulic performances of louvered and wavy finned heat exchangers", *International Journal of Thermal Sciences*, Vol. 151, p. 106256.

Okbaz, A., Pinarbaşi, A., Olcay, A.B. and Aksoy, M.H. (2018), "An experimental, computational and flow visualization study on the air-side thermal and hydraulic performance of louvered fin and round tube heat exchangers", *International Journal of Heat and Mass Transfer*, Vol. 121, pp. 153-169.

Pussoli, B.F., Barbosa, J.R., Jr, da Silva, L.W. and Kaviany, M. (2012), "Heat transfer and pressure drop characteristics of peripheral-finned tube heat exchangers", *International Journal of Heat and Mass Transfer*, Vol. 55 Nos 11/12, pp. 2835-2843.

Ribeiro, G.B. and Barbosa, J.R. Jr. (2019), "Use of peripheral fins for R-290 charge reduction in split-type residential air-conditioners", *International Journal of Refrigeration*, Vol. 106, pp. 1-6.

Schmidt, T.E. (1949), "Heat transfer calculations for extended surfaces", *Refrigerating Engineering*, Vol. 57, pp. 351-357.

Sertkaya, A.A., Altınısık, K. and Dincer, K. (2012), "Experimental investigation of thermal performance of aluminum finned heat exchangers and open-cell aluminum foam heat exchangers", *Experimental Thermal and Fluid Science*, Vol. 36, pp. 86-92.

Shah, R.K. (1978), "Compact heat exchanger surface selection methods", *6th international heat transfer conference, Toronto*, 7-11 August, pp. 193-199.

Singh, S., Verma, P. and Ghosh, S.K. (2021), "Numerical and experimental analysis of performance in a compact plate heat exchanger using graphene oxide/water nanofluid", *International Journal of Numerical Methods for Heat and Fluid Flow*, Vol. 31 No. 11, pp. 3356-3372.

Sundén, B. (2010), "Simulation of compact heat exchanger performance", *International Journal of Numerical Methods for Heat and Fluid Flow*, Vol. 20 No. 5, pp. 551-569.

Tao, W.Q., He, Y.L. and Chen, L. (2019), "A comprehensive review and comparison on heatline concept and field synergy principle", *International Journal of Heat and Mass Transfer*, Vol. 135, pp. 436-459.

Tian, J., Kim, T., Lu, T.J., Hodson, H.P., Queheillalt, D.T., Sypeck, D.J. and Wadley, H.N.G. (2004), "The effects of topology upon fluid-flow and heat-transfer within cellular copper structures", *International Journal of Heat and Mass Transfer*, Vol. 47 Nos 14/16, pp. 3171-3186.

Umer, R., Barsoum, Z., Jishi, H., Ushijima, K. and Cantwell, W. (2018), "Analysis of the compression behaviour of different composite lattice designs", *Journal of Composite Materials*, Vol. 52 No. 6, pp. 715-729.

Vafai, K. and Tien, C.L. (1982), "Boundary and inertia effects on convective mass transfer in porous media", *International Journal of Heat and Mass Transfer*, Vol. 25 No. 8, pp. 1183-1190.

Välikangas, T., Singh, S., Sørensen, K. and Condra, T. (2018), "Fin-and-tube heat exchanger enhancement with a combined herringbone and vortex generator design", *International Journal of Heat and Mass Transfer*, Vol. 118, pp. 602-616.

Vazifeshenas, Y., Sedighi, K. and Shakeri, M. (2020), "Open cell metal foam as extended coolant surface – fuel cell application", *Fuel Cells*, Vol. 20 No. 2, pp. 108-115.

Wan, T., Liu, Y., Zhou, C., Chen, X. and Li, Y. (2021), "Fabrication, properties, and applications of open-cell aluminum foams: a review", *Journal of Materials Science and Technology*, Vol. 62, pp. 11-24.

Wan, R., Wang, Y., Kavtaradze, R., Ji, H. and He, X. (2020), "Research on the air-side thermal hydraulic performance of louvered fin and flat tube heat exchangers under low-pressure environment", *Experimental Heat Transfer*, Vol. 33 No. 1, pp. 81-99.

Wang, C.C., Chi, K.Y. and Chang, C.J. (2000), "Heat transfer and friction characteristics of plain fin-and-tube heat exchangers, part II: correlation", *International Journal of Heat and Mass Transfer*, Vol. 43 No. 15, pp. 2693-2700.

Wang, C.C., Hwang, Y.M. and Lin, Y.T. (2002), "Empirical correlations for heat transfer and flow friction characteristics of herringbone wavy fin-and-tube heat exchangers", *International Journal of Refrigeration*, Vol. 25 No. 5, pp. 673-680.

Webb, R.L. (1980), "Air-side heat transfer in finned tube heat exchangers", *Heat Transfer Engineering*, Vol. 1 No. 3, pp. 33-49.

Webb, R.L. and Kim, N.H. (2005), *Principles of Enhanced Heat Transfer*, Taylor and Francis, New York, NY.

Wu, Z., Caliot, C., Flamant, G. and Wang, Z. (2011), "Numerical simulation of convective heat transfer between air flow and ceramic foams to optimise volumetric solar air receiver performances", *International Journal of Heat and Mass Transfer*, Vol. 54 Nos 7/8, pp. 1527-1537.

Xu, H., Wang, Y. and Han, X. (2020), "Analytical considerations of thermal storage and interface evolution of a PCM with/without porous media", *International Journal of Numerical Methods for Heat and Fluid Flow*, Vol. 30 No. 1, pp. 373-400.

Yakhot, V., Orszag, S.A., Thangam, S., Gatski, T.B. and Speziale, C.G. (1992), "Development of turbulence models for shear flows by a double expansion technique", *Physics of Fluids A: Fluid Dynamics*, Vol. 4 No. 7, pp. 1510-1520.

Yan, H., Yang, X., Lu, T. and Xie, G. (2017), "Convective heat transfer in a lightweight multifunctional sandwich panel with X-type metallic lattice core", *Applied Thermal Engineering*, Vol. 127, pp. 1293-1304.

Yang, X., Wei, P., Cui, X., Jin, L. and He, Y.L. (2019), "Thermal response of annuli filled with metal foam for thermal energy storage: an experimental study", *Applied Energy*, Vol. 250, pp. 1457-1467.

Yu, Q., Straatman, A.G. and Thompson, B.E. (2006), "Carbon-foam finned tubes in air–water heat exchangers", *Applied Thermal Engineering*, Vol. 26 Nos 2/3, pp. 131-143.

Yu, Z.Q., Wang, P., Zhou, W.J., Li, Z.Y. and Tao, W.Q. (2018), "Study on the consistency between field synergy principle and entransy dissipation extremum principle", *International Journal of Heat and Mass Transfer*, Vol. 116, pp. 621-634.

Zhang, X., Jin, X., Xie, G. and Yan, H. (2017), "Thermo-fluidic comparison between sandwich panels with tetrahedral lattice cores fabricated by casting and metal sheet folding", *Energies*, Vol. 10 No. 7, p. 906.

Zhao, X.E.J., Zhang, Z., Chen, J., Liao, G., Zhang, F., Leng, E., Han, D. and Hu, W. (2020), "A review on heat enhancement in thermal energy conversion and management using field synergy principle", *Applied Energy*, Vol. 257, p. 113995.

Zhi, C., Du, S., Zhao, F., Li, J. and Liu, Y. (2021), "Prediction and analysis of thermal-hydraulic performance with slit fins in small diameter (3 mm to 4 mm) heat exchangers", *International Communications in Heat and Mass Transfer*, Vol. 129, p. 105684.

Zhu, X.W. and Zhao, J.Q. (2016), "Improvement in field synergy principle: more rigorous application, better results", *International Journal of Heat and Mass Transfer*, Vol. 100, pp. 347-354.

Corresponding author
Bengt Ake Sunden can be contacted at: bengt.sunden@energy.lth.se